New Distortional Buckling Design Rules for Slotted Perforated Cold-Formed Steel Beams

Natalia Degtyareva
Institute of Architecture and Construction, South Ural State University,
Chelyabinsk, Russia
Perampalam Gatheeshgar
Faculty of Engineering and Environment, University of Northumbria,
Newcastle, UK.

Keerthan Poologanathan
Faculty of Engineering and Environment, University of Northumbria,
Newcastle, UK.
Shanmuganathan Gunalan
School of Engineering and Built Environment, Griffith University,
Gold Coast, QLD, 4222, Australia.

Konstantinos Daniel Tsavdaridis
School of Civil Engineering, Faculty of Engineering, University of Leeds
Leeds, UK.

Stephen Napper
Faculty of Engineering and Environment, University of Northumbria,
Newcastle, UK.

Abstract

Cold-Formed Steel (CFS) members with slotted perforations in webs are used in civil construction to amplify the thermal and energy performance of structures. However, the slotted webs reduce the structural performance of the element, prominently their shear, bending and combined bending and shear strengths. Many research studies have been undertaken to examine the behaviour of CFS channel sections subject to bending. Yet, no research has been performed to investigate the distortional buckling behaviour of slotted perforated CFS flexural members. Finite Element (FE) models of CFS channels with staggered slotted perforations were developed herein to investigate their distortional buckling under bending stress. A parametric study was conducted in detail by developing 432 slotted perforated CFS FE models based on the validation process with available experimental results. In particular, this paper presents the FE analysis details of CFS flexural members with slotted perforations subject to distortional buckling and results. The reliability of the current Direct Strength Method (DSM) for CFS flexural members with web holes subject to distortional buckling in accordance with the North American Specification (AISI S100) (2016) and the Australian/New Zealand

Standards (AS/NZ 4600) (2018) was investigated. Modified DSM formulae for slotted perforated CFS flexural members subject to distortional buckling were also proposed.

Keywords: Cold-formed steel; Beam with Staggered Slotted Perforations; Ultimate Bending Capacity; Finite Element Analyses; Direct Strength Method; Distortional Buckling

1 Introduction

Cold-Formed Steel (CFS) members have been extensively employed as load-bearing structural members in low to mid-rise residential and commercial buildings and modular building constructions. The advancements achieved in CFS manufacturing technologies have led to modifications in CFS profiles. One such modification is CFS channels with staggered slotted perforations (see Fig. 1). These slotted perforated channels have been preferred in light gauge steel constructions to amplify the overall thermal, energy and fire performances [1-4]. The aforementioned performance enhancements are achieved from the presence of staggered slotted perforations in the web of CFS profiles which interrupt the direct heat flow path as depicted in Fig. 2. Therefore, staggered slotted perforated CFS channels have proven their promising advantages over solid web CFS channels and applicability in construction [1-4] (see Fig. 3). However, the structural performance of these types of channels needs to be examined thoroughly as the web perforations are more sensitive to the ultimate load-bearing capacities of the CFS channels.

Previous studies have focused on investigating the compression, shear, and combined bending and shear behaviour of slotted perforated CFS wall studs and beams. Kesti [5] performed research on local and distortional buckling behaviour of slotted perforated wall studs and proposed suitable design guidelines. The shear behaviour of slotted perforated CFS channels has been investigated through structural tests [6] and numerical modelling [7] and it was found that the ultimate shear capacity was reduced up to 70% due to the presence of slotted perforations in the web. Degtyreva et al. [8] investigated the combined bending and shear behaviour of slotted perforated CFS channels through the numerical analysis and presented design proposals to predict the combined bending and shear capacity. Numerous experimental and numerical research studies have been performed to study the flexural behaviour of C-sections, Z-sections, and hollow flange sections with solid webs [9-16]. In addition, flexural behaviour of CFS beams with conventional shape web holes have also been studied [17, 18] and the Direct Strength Method (DSM) based design equations have been modified to consider the effect of web holes on ultimate bending capacity. However, no research has been conducted on the distortional and local buckling behaviours of CFS flexural members with staggered slotted web perforations to date, except some review about experimental studies in [19, 20]. Hence, detailed research is carried out herein to assess the distortional buckling behaviour of CFS flexural members with staggered slotted perforated webs.

Detailed information on the numerical studies of staggered slotted perforated CFS flexural members subject to distortional buckling is presented. Initially, CFS solid, rectangular web hole, and slotted web elements were modelled and the results were compared with the available experimental data to verify the model. Subsequently, a wide range of parametric studies was conducted and the results were used to extend the DSM based distortional buckling design equations for stagged slotted perforated CFS flexural members.

2 Finite element modelling description and verification

The numerical models, with material and geometric nonlinearities, were constructed and analysed using a general-purpose Finite Element (FE) software, ANSYS [21]. FE specimen models were developed as simply supported four-point loading arrangement to ensure pure bending failure. Because of the symmetric nature of the loading arrangement, only half of the beam was modelled. FE models were analysed in two stages, linear elastic buckling analysis, and non-linear analysis, successively. The reported study utilized the supercomputer resources of South Ural State University. The supercomputer resources are the distributed memory parallel computers which resulted in a time efficiency of the performed FE analysis. The following sub-sections elaborate the detailed description on the FE model development.

2.1 Material modelling

The non-linearity of the material in CFS beams was modelled with von Mises yield criteria along with isotropic hardening. The model consists of two components which are CFS channels and Web Side Plates (WSPs). The thin-walled CFS channel and 5 mm thickness of WSPs were modelled as bi-linear isotropic hardening (elastic-perfectly plastic) and elastic material, respectively. The modulus of the elasticity of the material is considered as 200 GPa, the Poisson's ratio was taken as 0.3 for both CFS channels and WSP. In general practice, both residual stresses and corner strength enhancements countereffect each other. Hence, both effects were not considered in the FE model development [22].

2.2 Element types

SHELL 181 element available in ANSYS [21] was used to model the CFS channels and WSPs. This SHELL181 element has four nodes and each node is controlled with three translational and three rotational degrees of freedom. This element is well-suited to simulate linear, large rotation and large strain non-linear problems, thus can result in accurate predictions accounting geometrical and material non-linearity of thin-walled CFS channels. The contact between WSP and CFS channel was modelled with CONTA173 and TARGE170 elements.

2.3 Mesh control

The CFS channels and WSPs were meshed with quadrilateral element shapes. For greater accuracy and efficiency of computing time, the solid segments (non-perforated regions) were refined with a maximum mesh size of 5 mm × 5 mm. However, the slotted perforated regions were provided with 1.5 mm × 5 mm mesh refinement, where 1.5 mm of maximum element size in the vertical direction and 5 mm maximum element size in the longitudinal direction in the perforated region. Similar mesh refinements were also used to study the shear [7] and combined bending and shear [8] behaviour of slotted perforated CFS channels. Fig. 4 shows the details of mesh refinements used in solid and slotted channels.

2.4 Geometric imperfections

The ultimate strength prediction and post-buckling behaviour of CFS thin-walled members hugely rely on initial geometric imperfections [23]. Therefore, the inclusion of geometric imperfections into the FE model is necessary. To account this, the imperfection shape and magnitude were incorporated to the FE models via super positioning buckling modes which were obtained from eigenvalue buckling analysis. The distortional buckling modes obtained in elastic buckling analysis were selected to add the imperfection. The general form of imperfection magnitude is given as a function of plate thickness or plate slenderness. Since the main focus of this paper is to investigate the distortional buckling behaviour of CFS flexural members with slotted perforations, imperfection magnitudes of 0.94t, 0.64t, and 0.15t (t = plate thickness) were used as proposed in [23, 24]. Detailed description on the imperfections can be found in the following sections.

2.5 Boundary conditions

Four-point loading simply supported boundary conditions were provided to the FE model. The boundary conditions given to the CFS channels in the validation process are depicted in Figs. 5-7. Only half of the test set-up was simulated due to the symmetric nature of the four-point loading bending test arrangement. The WSPs were the target surface and the CFS channels were the contact surface. All the WSP nodes were restrained in the x-direction at the support and loading point. The WSPs were connected to the CFS channels at the bolt locations through coupling the WSP and CFS channel nodes in x-, y-, and z-directions. Strap locations were simulated as boundary conditions by restraining the translation in the x-direction and the rotation in the z-direction. The translation of the support WSP in y-direction was restrained at the middle node of the bottom edge of the WSP. The nodes located at top edge of the loading WSP were also coupled in the y-direction. The load was applied to the coupled node, where all the vertical displacements are coupled, as displacement control approach.

2.6 Analysis procedure

The entire solution scheme has two phases: the elastic eigenvalue buckling analysis, and the non-linear analysis. Initially, elastic eigenvalue buckling analysis was performed to the developed FE models to generate the possible buckling modes. From that, the lowest distortional buckling mode was used to input the shape and magnitude of the initial geometric imperfection for non-linear analysis. The non-linear static analysis was used to obtain the ultimate bending capacity subject to distortional buckling and the failure mode. This non-linear analysis allows material yielding and large deformations when CFS beam subjected to loading thus produces accurate results. The non-linear analysis was performed through sparse direct equation solver.

2.7 FE Model verification

FE models were developed and verified against the available experiment results to ensure the considered model characteristics are suitable for further study. Distortional buckling test results of six solid web channels [25], three solid CFS channels and six CFS channels with rectangular unstiffened web holes [17], and five CFS beams with slotted perforations [19] were used to validate the FE models. Distortional buckling failure in the mid-span (pure bending zone) of the four-point loading set-up was achieved by unrestraining the lateral translation of the compression flange of CFS channels. Fig 4 shows the developed FE models for the validation against test results while Figs. 5, 6 and 7 depict the provided boundary conditions to simulate the actual test boundary conditions used in [25], [17] and [19] respectively. During this verification process, three different imperfection magnitudes (0.94t, 0.64t, and 0.15t, where t = plate thickness) with positive and negative values were used to determine the ultimate capacity of the FE models. These positive and negative values represent the associated distortional buckling modes of inward and outward movement of the top flange-lip juncture. Table 1, Table 2 and Table 3 present the comparisons of the ultimate bending capacity results subjected to distortional buckling failure obtained from the experiments (reported in [25], [17] and [19] respectively) and FE analyses. Overall comparison of the test results and FE analysis bending capacity predicted with different imperfection magnitude is provided in Table 4. From Table 4, it can be noticed that the mean values of the test to FE ultimate capacity ratio for all 20 specimens show satisfactory agreement. Even though the imperfections were not measured during the past distortional buckling tests [25, 17, 19] which are used for validation, the selected imperfections magnitudes (0.15t, 0.64t and 0.94t) based on the proposals made by Schafer and Pekoz [23] and Camotim and Silvestre [24] suited well to use in FE modelling. Moreover, the selected imperfection magnitudes are within the manufacturing limits. Similar imperfection magnitudes were also used in past research studies [13, 26]. To elaborate, it provides a mean value of 1.03, 1.06, 1.02, 1.04, 0.98, and 0.98 for imperfection magnitudes of 0.94t, -0.94t, 0.64t,-0.64t, 0.15t, and -0.15t, respectively. In addition to that the coefficient of variation (COV) values are 0.07 for 0.94t , 0.06 for -0.94t, 0.64t, -0.64t, and 0.15t, and 0.08 for -0.15t imperfection magnitudes.

Table 1: Comparison of FE results and experimental [25] bending capacities of solid CFS channels

Sections	Test (kNm)	FE results for different imperfection magnitudes											
		0.94t		-0.94t		0.64t		-0.64t		0.15t		-0.15t	
		FE (kNm)	Test / FE	FE (kNm)	Test / FE	FE (kNm)	Test / FE	FE (kNm)	Test / FE	FE (kNm)	Test / FE	FE (kNm)	Test / FE
C15015-Mw	9.47	9.97	0.95	8.91	1.06	9.90	0.96	9.04	1.05	9.61	0.99	9.44	1.00
C15019-Mw	12.94	12.51	1.03	11.78	1.10	12.95	1.00	12.05	1.07	13.51	0.96	12.81	1.01
C15024-Mw	17.76	16.21	1.10	15.19	1.17	16.36	1.09	15.50	1.15	16.70	1.06	16.11	1.10
C20015-Mw	12.20	11.95	1.02	10.66	1.14	11.82	1.03	10.91	1.12	11.75	1.04	11.53	1.06
C20019-Mw	18.85	17.35	1.09	16.70	1.13	18.60	1.01	17.32	1.09	19.04	0.99	18.39	1.03
C20024-Mw	27.88	26.46	1.05	24.54	1.14	27.33	1.02	24.92	1.12	26.22	1.06	25.66	1.09
Min			0.95		1.06		0.96		1.05		0.96		1.00
Max			1.10		1.17		1.09		1.15		1.06		1.10
Mean			1.04		1.12		1.02		1.10		1.02		1.05
COV			0.05		0.03		0.04		0.03		0.04		0.04

Note: t = thickness

Table 2: Comparison of FE results and experimental [17] bending capacities of solid and rectangular web holed CFS channels

Sections	Test (kNm)	FE results for different imperfection magnitudes											
		0.94t		-0.94t		0.64t		-0.64t		0.15t		-0.15t	
		FE (kNm)	Test / FE	FE (kNm)	Test / FE	FE (kNm)	Test / FE	FE (kNm)	Test / FE	FE (kNm)	Test / FE	FE (kNm)	Test / FE
NH-1.1	12.6	12.06	1.05	12.06	1.04	12.15	1.04	12.35	1.02	13.52	0.93	14.42	0.87
NH-2.1	12.51	11.71	1.07	11.71	1.07	11.82	1.06	12.00	1.04	13.31	0.94	13.86	0.90
NH-3.2	13.02	11.92	1.09	11.92	1.09	12.03	1.08	12.21	1.07	13.49	0.97	14.19	0.92
H0.9-1.1	9.65	9.17	1.05	9.33	1.03	9.27	1.04	9.52	1.01	10.03	0.96	10.49	0.92
H0.9-2.2	10.54	9.58	1.10	9.83	1.07	9.76	1.08	10.12	1.04	11.29	0.93	11.62	0.91
H0.9-3.1	10.84	9.77	1.11	10.00	1.08	9.94	1.09	10.32	1.05	11.49	0.94	11.88	0.91
H0.8-1.2	8.19	8.34	0.98	8.44	0.97	8.55	0.96	8.63	0.95	9.03	0.91	9.20	0.89
H0.8-2.2	8.55	8.34	1.03	8.44	1.01	8.55	1.00	8.63	0.99	9.01	0.95	9.18	0.93
H0.8-3.2	8.56	8.53	1.00	8.62	0.99	8.73	0.98	8.81	0.97	9.25	0.93	9.38	0.91
Min			0.98		0.97		0.96		0.95		0.91		0.87
Max			1.11		1.09		1.09		1.07		0.97		0.93
Mean			1.05		1.04		1.04		1.02		0.94		0.91
COV			0.04		0.04		0.05		0.04		0.02		0.02

Note: t = thickness

Table 3: Comparison of FE results and experimental [19] bending capacities of slotted perforated CFS channels

Sections	Test (kNm)	FE results for different imperfection magnitudes											
		0.94t		-0.94t		0.64t		-0.64t		0.15t		-0.15t	
		FE (kNm)	Test / FE	FE (kNm)	Test / FE	FE (kNm)	Test / FE	FE (kNm)	Test / FE	FE (kNm)	Test / FE	FE (kNm)	Test / FE
PA-145-1.0	2.65	2.99	0.89	2.83	0.94	3.03	0.88	2.85	0.93	2.91	0.91	2.91	0.91
PA-145-1.5	5.42	5.72	0.95	5.00	1.08	5.78	0.94	5.08	1.07	5.40	1.00	5.19	1.04
PA-195-1.0	3.92	3.58	1.10	3.93	1.00	3.73	1.05	3.95	0.99	3.68	1.06	4.00	0.98
PA-195-1.5	6.80	7.58	0.90	6.58	1.03	6.81	1.00	6.61	1.03	7.59	0.90	6.67	1.02
PA-195-1.3	4.22	3.87	1.09	4.29	0.98	3.79	1.11	3.81	1.11	3.83	1.10	3.82	1.11
Min			0.89		0.94		0.88		0.93		0.90		0.91
Max			1.10		1.08		1.11		1.11		1.10		1.11
Mean			0.98		1.01		1.00		1.03		1.00		1.01
COV			0.10		0.05		0.09		0.07		0.09		0.07

Note: t = thickness

Table 4: Overall comparison of FE results and experimental [25, 17, 19] bending capacities of CFS channels

Sections	Overall Test /FE ratios for different imperfection magnitudes					
	Test/ $FE_{(0.94t)}$	Test/ $FE_{(-0.94t)}$	Test/ $FE_{(0.64t)}$	Test/ $FE_{(-0.64t)}$	Test/ $FE_{(0.15t)}$	Test/ $FE_{(-0.15t)}$
Min	0.89	0.94	0.88	0.93	0.90	0.87
Max	1.11	1.17	1.11	1.15	1.10	1.11
Mean	1.03	1.06	1.02	1.04	0.98	0.98
COV	0.07	0.06	0.06	0.06	0.06	0.08

Note: t = thickness

During the tests, the vertical displacement of the midpoint of the beam span was measured with the application of load. Similarly, in FE models the displacement of the midpoint of the beam span was obtained to ensure the test and FE deformations can be compared. Fig. 8 depicts the failure mode comparison between the FE analysis and test [26] for 150 mm deep channel with

1.9 mm thickness and without straps (C15019-Mw) while Fig. 9 shows the load-vertical displacement behaviour obtained for the specimen C15019-Mw from the experiment [25] and FE analysis. Both test and FE modelling load-vertical displacement have shown almost linear response in Fig. 9 as this CFS section is relatively slender. In addition, this can cause sudden elastic distortional buckling failure in mid-span. The aforementioned behaviour was observed in tests by Pham and Hancock [25] and FE analysis in this study (see Fig. 8). This confirms that the non-linear response is more likely to happen in stocky sections. The load-vertical displacement behaviour for C15019-Mw shows consistent results at each stage in FE analysis and test. The failure modes also depicted a high similarity between FE analysis and test. Moreover, failure modes comparison between the test [17] and FE analysis for the specimens with rectangular web openings is illustrated in Fig. 10. This comparison also showed similar failure modes obtained in both cases of test and FE analysis. Overall, FE results for the CFS flexural members which fail under distortional buckling agree well with that of the test results in terms of (a) ultimate bending capacity; (b) load-vertical displacement behaviour and (c) failure modes. This confirms that similar FE models characteristics including element types, material model, and analysis type can be used to perform the parametric studies of CFS flexural members with staggered slotted perforations subject to distortional buckling.

3 Parametric studies

This section presents the FE model details of the parametric study which was conducted to investigate the distortional buckling failure behaviour of CFS flexural members. The parametric study was aimed to create a wide range of data set and to develop improved design guidelines to predict the ultimate bending capacity of CFS beams with staggered slotted perforations subject to distortional buckling.

3.1 Varying parameters

After the validation process, a parametric study was conducted to create a wide range of results base which can cover wider bounds. Therefore, the improved formula could be able to predict the distortional buckling ultimate bending capacity of the staggered slotted perforated CFS beams with different dimensional and mechanical properties. Therefore, section depth (D), Flange width (B_f) (constant for particular section depth (D)), thickness (t), slot length (L_{sl}), slot width (W_{sl}), number of slot rows (n), number of slot row groups (N) and yield strength (f_y) were varied. Three different section depths of 150, 200, and 250 mm, two different flange lengths of 45 and 65 mm, three different thicknesses of 1, 2, and 3 mm, two different slot length of 60 and 75 mm, two different slot widths of 3 and 5 mm, three different slot rows of 6, 8, and 12 (6 rows for 150 mm section depth, 6 and 8 rows for 200 mm section depth, and 6, 8, and 12 rows for 250 mm section depth) , two-slot row groups and three different yield strength of 300, 500, and 600 MPa were considered in the parametric study. The varying parameters are presented in Table 5. A total number of 432 FE models were developed and analysed for this parametric study considering the aforementioned influencing parameters. The labelling rule for the FE models developed for the parametric study is illustrated in Fig.11.

Table 5: Parametric study details

fy (MPa)	D (mm)	B_f (mm)	B_l (mm)	t (mm)	L_{sl} (mm)	W_{sl} (mm)	n	N	Number of models
300	150	45	13	1, 2, 3	60, 75	3, 5	6	1, 2	24
	200	45	13	1, 2, 3	60, 75	3, 5	6, 8	1, 2	48
	250	65	13	1, 2, 3	60, 75	3, 5	6, 8, 12	1, 2	72
Sub-total									144
500	150	45	13	1, 2, 3	60, 75	3, 5	6	1, 2	24
	200	45	13	1, 2, 3	60, 75	3, 5	6, 8	1, 2	48
	250	65	13	1, 2, 3	60, 75	3, 5	6, 8, 12	1, 2	72
Sub-total									144
600	150	45	13	1, 2, 3	60, 75	3, 5	6	1, 2	24
	200	45	13	1, 2, 3	60, 75	3, 5	6, 8	1, 2	48
	250	65	13	1, 2, 3	60, 75	3, 5	6, 8, 12	1, 2	72
Sub-total									144
Total									432

Note: fy = yield stress, D = section depth, B_f = flange width, B_l = lip length, t = thickness, L_{sl} = slot length, W_{sl} = slot width, n = number of slot rows, N = number of slot row groups

3.2 Selection of FE model span

The validated FE models have the total span of 2600, 4800, and 3950 mm as similar to test spans which were reported in [25], [17], and [19], respectively. For the parametric study, it is essential to select one span. Therefore, a few analyses were performed to evaluate the influence of the total span on the ultimate bending capacity of the CFS beams with staggered slotted perforations. For same dimensions of the CFS beams, the analysis was conducted in two options: (a) CFS beams having the span of 4800 mm and staggered slotted perforations incorporated in the entire web of the span (see Fig. 12); (b) CFS beams having the span of 2600 mm and staggered slotted perforations incorporated only in web of the mid-span (see Fig. 13). The boundary conditions used for these two options are depicted in Figs. 14 and 15, respectively. The ultimate bending capacity obtained from the FE analysis for these two cases were compared and the results are presented in Table 6. Figs. 16-18 shows the failure modes comparison obtained at different stages for these short and long span channels. The results showed that the span and providing slotted perforation in two end spans of the four-point loading arrangement do not influence the ultimate bending capacity. Therefore, the span of 2600 mm with staggered slotted perforations provided only in the mid-span (option (b)) was used for the parametric study because the shorter span consumes less computational time compared to the larger span and the solid shear span in the shorter beam prevents the combined bending and shear failure.

Moreover, Pham and Hancock [25] and Moen et al. [17] used different mid-span lengths of 1000 mm and 1626 mm, respectively in their four-point test set-ups. The performed analysis to investigate the influence of the total span of the four-point set-up also confirm the different lengths for mid-span (option (a): mid-span is 1626 mm, and option (b): mid-span is 1000 mm) have no influence on the ultimate bending capacity prediction. Hence, the consideration of the ratio between mid-span and the distortional buckling half wavelength is likely to be neglected.

Table 6: FE ultimate bending capacity comparison for slotted CFS channels having different spans.

FE model	$M_{slots, 4.8}$ (kNm)	$M_{slots, 2.6}$ (kNm)	$M_{slots, 4.8}/M_{slots, 2.6}$
150-1-60-3-1-6-600	3.88	3.85	1.01
150-1-60-3-2-6-600	3.47	3.44	1.01
150-3-60-3-1-6-600	16.02	15.94	1.01
150-3-60-3-2-6-600	15.45	15.35	1.01
250-1-60-3-1-6-600	6.22	6.20	1.00
250-1-60-3-2-6-600	6.16	6.15	1.00
250-1-60-3-1-12-600	6.04	6.06	1.00
250-1-60-3-2-12-600	5.79	5.76	1.00
250-3-60-3-1-6-600	36.11	36.02	1.00
250-3-60-3-2-6-600	35.59	35.56	1.00
250-3-60-3-1-12-600	34.77	34.74	1.00
250-3-60-3-2-12-600	33.41	33.36	1.00
150-1-60-3-1-6-300	2.74	2.73	1.00
150-1-60-3-2-6-300	2.57	2.58	1.00
150-3-60-3-1-6-300	9.23	9.20	1.00
150-3-60-3-2-6-300	9.05	9.00	1.01
250-1-60-3-1-6-300	4.81	4.80	1.00
250-1-60-3-2-6-300	4.73	4.79	0.99
250-1-60-3-1-12-300	4.63	4.65	1.00
250-1-60-3-2-12-300	4.42	4.40	1.01
250-3-60-3-1-6-300	22.15	22.10	1.00
250-3-60-3-2-6-300	21.82	21.81	1.00
250-3-60-3-1-12-300	21.35	21.33	1.00
250-3-60-3-2-12-300	20.71	20.72	1.00

Note: $M_{slots, 4.8}$ = bending capacity for 4800 mm span, $M_{slots, 2.6}$ = bending capacity for 2600 mm span

4 Results analysis of the parametric study

The flexural behaviour of CFS beams with staggered slotted perforations was investigated in detail using 432 FE parametric models. In addition to that the bending capacity of the corresponding solid web channels (without slotted perforations) were also obtained from FE as a reference and those results were required to propose improved design guidelines as explained in following sections. Figs 19a and 19b show the von Mises stress failure modes of the 150 mm section depth CFS solid web channels and the corresponding failure modes when staggered slotted perforations are provided. In addition to that deformation failure patterns obtained from the FE analysis for the staggered slotted perforated CFS channels are depicted in Fig. 20. Table 7 summarises the distortional buckling moments, section and elastic properties of the solid web channels. The entire parametric study results of bending capacity for the staggered slotted perforations and the corresponding capacities for the solid CFS channels are presented in Table 8-10 for 300, 500, and 600 MPa yield strengths, respectively. Here M_{solid} is the flexural capacity of the solid CFS channels and the M_{slots} is the flexural capacity of the staggered slotted channels subjected to distortional buckling. The reduction factor, which is the ratio between the bending capacity of the staggered slotted channel and the corresponding bending capacity of the solid CFS channel are also presented in Table 8-10 for all 432 Fe models. Overall, it can be noticed up to 23% of bending capacity reduction was noticed and this occurs when web experiences the highest web area reduction. The small capacity reduction was noticed when the CFS channel web experiences the lowest area reduction due to the slotted perforations. Moreover, CFS channels with two-row groups of slotted perforations resulted in a higher bending capacity reduction than similar CFS channels with single row groups of slotted perforations when other parameters remain the same. This behaviour can be argued that the slotted perforations are subjected to higher compressive stress as the slots are placed near the compression flange in the case of two slot row groups, but near the neutral axis in the case of single-slot row group. The variation of the reduction factor against the considered influencing parameters is plotted in Fig. 21.

Table 7: Section and elastic properties of the solid web CFS channels

D (mm)	B_f (mm)	B_l (mm)	t (mm)	Z (mm^3)	S (mm^3)	S/Z	M_{od} (kNm)	λ_d		
								fy=300 MPa	fy=500 MPa	fy=600 MPa
150	45	13	1	11 416	13 812	1.21	3.52	0.99	1.27	1.39
			2	21 416	26 945	1.26	15.12	0.65	0.84	0.92
			3	30 024	39 404	1.31	37.16	0.49	0.64	0.70
200	45	13	1	17 018	20 987	1.23	3.81	1.16	1.49	1.64
			2	32 199	41 094	1.28	16.90	0.76	0.98	1.07
			3	45 567	60 329	1.32	43.39	0.57	0.73	0.80
250	65	13	1	28 416	34 393	1.21	3.65	1.51	1.95	2.14
			2	54 495	67 644	1.24	16.38	0.99	1.28	1.40
			3	78 260	99 824	1.28	41.74	0.75	0.97	1.06
Mean						1.26				

Note: D = section depth, B_f = flange width, B_l = lip length, Z = elastic section modulus, S = plastic section modulus, M_{od} = distortional buckling moment, λ_d = distortional buckling slenderness based on yield and distortional buckling moment

Table 8: Parametric study results for f_y = 300 MPa

No	Channels with Slotted Webs	M_{slots} (kNm)	M_{solid} (kNm)	M_{slots} / M_{solid}	No	Channels with Slotted Webs	M_{slots} (kNm)	M_{solid} (kNm)	M_{slots} / M_{solid}
1	150-1-60-3-1-6-300	2.73	2.95	0.93	73	250-1-60-3-1-6-300	4.82	4.93	0.98
2	150-1-60-5-1-6-300	2.66	2.95	0.90	74	250-1-60-5-1-6-300	4.83	4.93	0.98
3	150-1-75-3-1-6-300	2.64	2.95	0.90	75	250-1-75-3-1-6-300	4.80	4.93	0.97
4	150-1-75-5-1-6-300	2.55	2.95	0.87	76	250-1-75-5-1-6-300	4.72	4.93	0.96
5	150-1-60-3-2-6-300	2.58	2.95	0.88	77	250-1-60-3-2-6-300	4.79	4.93	0.97
6	150-1-60-5-2-6-300	2.40	2.95	0.82	78	250-1-60-5-2-6-300	4.74	4.93	0.96
7	150-1-75-3-2-6-300	2.44	2.95	0.83	79	250-1-75-3-2-6-300	4.72	4.93	0.96
8	150-1-75-5-2-6-300	2.30	2.95	0.78	80	250-1-75-5-2-6-300	4.68	4.93	0.95
9	150-2-60-3-1-6-300	6.09	6.44	0.95	81	250-1-60-3-1-8-300	4.80	4.93	0.97
10	150-2-60-5-1-6-300	5.99	6.44	0.93	82	250-1-60-5-1-8-300	4.76	4.93	0.97
11	150-2-75-3-1-6-300	5.96	6.44	0.93	83	250-1-75-3-1-8-300	4.74	4.93	0.96
12	150-2-75-5-1-6-300	5.86	6.44	0.91	84	250-1-75-5-1-8-300	4.66	4.93	0.94
13	150-2-60-3-2-6-300	5.90	6.44	0.92	85	250-1-60-3-2-8-300	4.71	4.93	0.95
14	150-2-60-5-2-6-300	5.75	6.44	0.89	86	250-1-60-5-2-8-300	4.68	4.93	0.95
15	150-2-75-3-2-6-300	5.80	6.44	0.90	87	250-1-75-3-2-8-300	4.60	4.93	0.93
16	150-2-75-5-2-6-300	5.64	6.44	0.88	88	250-1-75-5-2-8-300	4.52	4.93	0.92
17	150-3-60-3-1-6-300	9.20	9.53	0.96	89	250-1-60-3-1-12-300	4.65	4.93	0.94
18	150-3-60-5-1-6-300	9.10	9.53	0.95	90	250-1-60-5-1-12-300	4.60	4.93	0.93
19	150-3-75-3-1-6-300	9.42	9.53	0.99	91	250-1-75-3-1-12-300	4.57	4.93	0.93
20	150-3-75-5-1-6-300	9.32	9.53	0.98	92	250-1-75-5-1-12-300	4.49	4.93	0.91
21	150-3-60-3-2-6-300	9.00	9.53	0.94	93	250-1-60-3-2-12-300	4.40	4.93	0.89
22	150-3-60-5-2-6-300	8.83	9.53	0.93	94	250-1-60-5-2-12-300	4.36	4.93	0.88
23	150-3-75-3-2-6-300	9.22	9.53	0.97	95	250-1-75-3-2-12-300	4.31	4.93	0.87
24	150-3-75-5-2-6-300	9.03	9.53	0.95	96	250-1-75-5-2-12-300	4.23	4.93	0.86
25	200-1-60-3-1-6-300	3.86*	3.86	1.00	97	250-2-60-3-1-6-300	13.61	13.70	0.99
26	200-1-60-5-1-6-300	3.81	3.86	0.99	98	250-2-60-5-1-6-300	13.54	13.70	0.99
27	200-1-75-3-1-6-300	3.74	3.86	0.97	99	250-2-75-3-1-6-300	13.48	13.70	0.98
28	200-1-75-5-1-6-300	3.69	3.86	0.96	100	250-2-75-5-1-6-300	13.34	13.70	0.97
29	200-1-60-3-2-6-300	3.68	3.86	0.95	101	250-2-60-3-2-6-300	13.42	13.70	0.98
30	200-1-60-5-2-6-300	3.63	3.86	0.94	102	250-2-60-5-2-6-300	13.38	13.70	0.98
31	200-1-75-3-2-6-300	3.60	3.86	0.93	103	250-2-75-3-2-6-300	13.31	13.70	0.97
32	200-1-75-5-2-6-300	3.54	3.86	0.92	104	250-2-75-5-2-6-300	13.21	13.70	0.96
33	200-1-60-3-1-8-300	3.72	3.86	0.96	105	250-2-60-3-1-8-300	13.48	13.70	0.98
34	200-1-60-5-1-8-300	3.67	3.86	0.95	106	250-2-60-5-1-8-300	13.41	13.70	0.98
35	200-1-75-3-1-8-300	3.75	3.86	0.97	107	250-2-75-3-1-8-300	13.32	13.70	0.97

36	200-1-75-5-1-8-300	3.71	3.86	0.96	108	250-2-75-5-1-8-300	13.19	13.70	0.96
37	200-1-60-3-2-8-300	3.56	3.86	0.92	109	250-2-60-3-2-8-300	13.22	13.70	0.97
38	200-1-60-5-2-8-300	3.48	3.86	0.90	110	250-2-60-5-2-8-300	13.16	13.70	0.96
39	200-1-75-3-2-8-300	3.45	3.86	0.89	111	250-2-75-3-2-8-300	13.12	13.70	0.96
40	200-1-75-5-2-8-300	3.33	3.86	0.86	112	250-2-75-5-2-8-300	13.00	13.70	0.95
41	200-2-60-3-1-6-300	8.87	9.03	0.98	113	250-2-60-3-1-12-300	13.11	13.70	0.96
42	200-2-60-5-1-6-300	8.77	9.03	0.97	114	250-2-60-5-1-12-300	13.01	13.70	0.95
43	200-2-75-3-1-6-300	8.69	9.03	0.96	115	250-2-75-3-1-12-300	12.95	13.70	0.95
44	200-2-75-5-1-6-300	8.56	9.03	0.95	116	250-2-75-5-1-12-300	12.75	13.70	0.93
45	200-2-60-3-2-6-300	8.61	9.03	0.95	117	250-2-60-3-2-12-300	12.68	13.70	0.93
46	200-2-60-5-2-6-300	8.51	9.03	0.94	118	250-2-60-5-2-12-300	12.36	13.70	0.90
47	200-2-75-3-2-6-300	8.44	9.03	0.93	119	250-2-75-3-2-12-300	12.44	13.70	0.91
48	200-2-75-5-2-6-300	8.31	9.03	0.92	120	250-2-75-5-2-12-300	11.96	13.70	0.87
49	200-2-60-3-1-8-300	8.70	9.03	0.96	121	250-3-60-3-1-6-300	22.13	22.66	0.98
50	200-2-60-5-1-8-300	8.59	9.03	0.95	122	250-3-60-5-1-6-300	22.02	22.66	0.97
51	200-2-75-3-1-8-300	8.50	9.03	0.94	123	250-3-75-3-1-6-300	22.56	22.66	0.99
52	200-2-75-5-1-8-300	8.36	9.03	0.93	124	250-3-75-5-1-6-300	22.38	22.66	0.99
53	200-2-60-3-2-8-300	8.37	9.03	0.93	125	250-3-60-3-2-6-300	21.84	22.66	0.96
54	200-2-60-5-2-8-300	8.26	9.03	0.91	126	250-3-60-5-2-6-300	21.69	22.66	0.96
55	200-2-75-3-2-8-300	8.20	9.03	0.91	127	250-3-75-3-2-6-300	22.22	22.66	0.98
56	200-2-75-5-2-8-300	8.09	9.03	0.90	128	250-3-75-5-2-6-300	22.02	22.66	0.97
57	200-3-60-3-1-6-300	13.80	13.86	1.00	129	250-3-60-3-1-8-300	22.01	22.66	0.97
58	200-3-60-5-1-6-300	13.73	13.86	0.99	130	250-3-60-5-1-8-300	21.81	22.66	0.96
59	200-3-75-3-1-6-300	13.96	13.86	1.01*	131	250-3-75-3-1-8-300	22.32	22.66	0.98
60	200-3-75-5-1-6-300	13.87	13.86	1.00*	132	250-3-75-5-1-8-300	22.07	22.66	0.97
61	200-3-60-3-2-6-300	13.60	13.86	0.98	133	250-3-60-3-2-8-300	21.52	22.66	0.95
62	200-3-60-5-2-6-300	13.50	13.86	0.97	134	250-3-60-5-2-8-300	21.34	22.66	0.94
63	200-3-75-3-2-6-300	13.74	13.86	0.99	135	250-3-75-3-2-8-300	21.87	22.66	0.97
64	200-3-75-5-2-6-300	13.56	13.86	0.98	136	250-3-75-5-2-8-300	21.62	22.66	0.95
65	200-3-60-3-1-8-300	13.66	13.86	0.99	137	250-3-60-3-1-12-300	21.38	22.66	0.94
66	200-3-60-5-1-8-300	13.58	13.86	0.98	138	250-3-60-5-1-12-300	21.12	22.66	0.93
67	200-3-75-3-1-8-300	13.75	13.86	0.99	139	250-3-75-3-1-12-300	21.61	22.66	0.95
68	200-3-75-5-1-8-300	13.63	13.86	0.98	140	250-3-75-5-1-12-300	21.28	22.66	0.94
69	200-3-60-3-2-8-300	13.37	13.86	0.96	141	250-3-60-3-2-12-300	20.74	22.66	0.92
70	200-3-60-5-2-8-300	13.21	13.86	0.95	142	250-3-60-5-2-12-300	20.40	22.66	0.90
71	200-3-75-3-2-8-300	13.39	13.86	0.97	143	250-3-75-3-2-12-300	20.96	22.66	0.92
72	200-3-75-5-2-8-300	13.20	13.86	0.95	144	250-3-75-5-2-12-300	20.42	22.66	0.90

Note: M_{slots} = bending capacity of slotted web channel, M_{solid} = bending capacity of solid web channel, * = numerical errors

Table 9: Parametric study results for f_y = 500 MPa

No	Channels with Slotted Webs	M_{slots} (kNm)	M_{solid} (kNm)	M_{slots} / M_{solid}	No	Channels with Slotted Webs	M_{slots} (kNm)	M_{solid} (kNm)	M_{slots} / M_{solid}
1	150-1-60-3-1-6-500	3.65	3.85	0.95	73	250-1-60-3-1-6-500	5.73	5.94	0.96
2	150-1-60-5-1-6-500	3.54	3.85	0.92	74	250-1-60-5-1-6-500	5.76	5.94	0.97
3	150-1-75-3-1-6-500	3.52	3.85	0.91	75	250-1-75-3-1-6-500	5.75	5.94	0.97
4	150-1-75-5-1-6-500	3.36	3.85	0.87	76	250-1-75-5-1-6-500	5.71	5.94	0.96
5	150-1-60-3-2-6-500	3.23	3.85	0.84	77	250-1-60-3-2-6-500	5.75	5.94	0.97
6	150-1-60-5-2-6-500	3.08	3.85	0.80	78	250-1-60-5-2-6-500	5.71	5.94	0.96
7	150-1-75-3-2-6-500	3.16	3.85	0.82	79	250-1-75-3-2-6-500	5.68	5.94	0.96
8	150-1-75-5-2-6-500	2.97	3.85	0.77	80	250-1-75-5-2-6-500	5.64	5.94	0.95
9	150-2-60-3-1-6-500	8.88	9.53	0.93	81	250-1-60-3-1-8-500	5.79	5.94	0.98
10	150-2-60-5-1-6-500	8.71	9.53	0.91	82	250-1-60-5-1-8-500	5.76	5.94	0.97
11	150-2-75-3-1-6-500	8.60	9.53	0.90	83	250-1-75-3-1-8-500	5.73	5.94	0.97
12	150-2-75-5-1-6-500	8.43	9.53	0.88	84	250-1-75-5-1-8-500	5.69	5.94	0.96
13	150-2-60-3-2-6-500	8.46	9.53	0.89	85	250-1-60-3-2-8-500	5.69	5.94	0.96
14	150-2-60-5-2-6-500	8.20	9.53	0.86	86	250-1-60-5-2-8-500	5.64	5.94	0.95
15	150-2-75-3-2-6-500	8.23	9.53	0.86	87	250-1-75-3-2-8-500	5.62	5.94	0.95

16	150-2-75-5-2-6-500	7.89	9.53	0.83	88	250-1-75-5-2-8-500	5.48	5.94	0.92
17	150-3-60-3-1-6-500	13.91	14.71	0.95	89	250-1-60-3-1-12-500	5.62	5.94	0.95
18	150-3-60-5-1-6-500	13.70	14.71	0.93	90	250-1-60-5-1-12-500	5.58	5.94	0.94
19	150-3-75-3-1-6-500	14.13	14.71	0.96	91	250-1-75-3-1-12-500	5.54	5.94	0.93
20	150-3-75-5-1-6-500	13.92	14.71	0.95	92	250-1-75-5-1-12-500	5.49	5.94	0.92
21	150-3-60-3-2-6-500	13.46	14.71	0.91	93	250-1-60-3-2-12-500	5.37	5.94	0.90
22	150-3-60-5-2-6-500	13.11	14.71	0.89	94	250-1-60-5-2-12-500	5.29	5.94	0.89
23	150-3-75-3-2-6-500	13.67	14.71	0.93	95	250-1-75-3-2-12-500	5.24	5.94	0.88
24	150-3-75-5-2-6-500	13.29	14.71	0.90	96	250-1-75-5-2-12-500	5.18	5.94	0.87
25	200-1-60-3-1-6-500	5.18	5.06	1.02*	97	250-2-60-3-1-6-500	18.92	19.09	0.99
26	200-1-60-5-1-6-500	5.12	5.06	1.01*	98	250-2-60-5-1-6-500	18.83	19.09	0.99
27	200-1-75-3-1-6-500	5.07	5.06	1.00*	99	250-2-75-3-1-6-500	18.68	19.09	0.98
28	200-1-75-5-1-6-500	5.01	5.06	0.99	100	250-2-75-5-1-6-500	18.61	19.09	0.97
29	200-1-60-3-2-6-500	4.97	5.06	0.98	101	250-2-60-3-2-6-500	18.79	19.09	0.98
30	200-1-60-5-2-6-500	4.90	5.06	0.97	102	250-2-60-5-2-6-500	18.69	19.09	0.98
31	200-1-75-3-2-6-500	4.88	5.06	0.96	103	250-2-75-3-2-6-500	18.61	19.09	0.97
32	200-1-75-5-2-6-500	4.75	5.06	0.94	104	250-2-75-5-2-6-500	18.49	19.09	0.97
33	200-1-60-3-1-8-500	5.01	5.06	0.99	105	250-2-60-3-1-8-500	18.89	19.09	0.99
34	200-1-60-5-1-8-500	4.95	5.06	0.98	106	250-2-60-5-1-8-500	18.72	19.09	0.98
35	200-1-75-3-1-8-500	5.08	5.06	1.00*	107	250-2-75-3-1-8-500	18.66	19.09	0.98
36	200-1-75-5-1-8-500	4.90	5.06	0.97	108	250-2-75-5-1-8-500	18.52	19.09	0.97
37	200-1-60-3-2-8-500	4.79	5.06	0.95	109	250-2-60-3-2-8-500	18.58	19.09	0.97
38	200-1-60-5-2-8-500	4.62	5.06	0.91	110	250-2-60-5-2-8-500	18.42	19.09	0.96
39	200-1-75-3-2-8-500	4.59	5.06	0.91	111	250-2-75-3-2-8-500	18.35	19.09	0.96
40	200-1-75-5-2-8-500	4.40	5.06	0.87	112	250-2-75-5-2-8-500	18.26	19.09	0.96
41	200-2-60-3-1-6-500	12.70	12.94	0.98	113	250-2-60-3-1-12-500	18.42	19.09	0.96
42	200-2-60-5-1-6-500	12.57	12.94	0.97	114	250-2-60-5-1-12-500	18.23	19.09	0.95
43	200-2-75-3-1-6-500	12.46	12.94	0.96	115	250-2-75-3-1-12-500	18.15	19.09	0.95
44	200-2-75-5-1-6-500	12.28	12.94	0.95	116	250-2-75-5-1-12-500	17.85	19.09	0.93
45	200-2-60-3-2-6-500	12.32	12.94	0.95	117	250-2-60-3-2-12-500	17.72	19.09	0.93
46	200-2-60-5-2-6-500	12.15	12.94	0.94	118	250-2-60-5-2-12-500	16.96	19.09	0.89
47	200-2-75-3-2-6-500	12.03	12.94	0.93	119	250-2-75-3-2-12-500	17.01	19.09	0.89
48	200-2-75-5-2-6-500	11.84	12.94	0.92	120	250-2-75-5-2-12-500	16.08	19.09	0.84
49	200-2-60-3-1-8-500	12.46	12.94	0.96	121	250-3-60-3-1-6-500	31.95	32.64	0.98
50	200-2-60-5-1-8-500	12.30	12.94	0.95	122	250-3-60-5-1-6-500	31.83	32.64	0.98
51	200-2-75-3-1-8-500	12.16	12.94	0.94	123	250-3-75-3-1-6-500	32.19	32.64	0.99
52	200-2-75-5-1-8-500	11.97	12.94	0.93	124	250-3-75-5-1-6-500	31.90	32.64	0.98
53	200-2-60-3-2-8-500	11.93	12.94	0.92	125	250-3-60-3-2-6-500	31.53	32.64	0.97
54	200-2-60-5-2-8-500	11.73	12.94	0.91	126	250-3-60-5-2-6-500	31.35	32.64	0.96
55	200-2-75-3-2-8-500	11.62	12.94	0.90	127	250-3-75-3-2-6-500	31.68	32.64	0.97
56	200-2-75-5-2-8-500	11.44	12.94	0.88	128	250-3-75-5-2-6-500	31.38	32.64	0.96
57	200-3-60-3-1-6-500	20.66	20.76	0.99	129	250-3-60-3-1-8-500	31.75	32.64	0.97
58	200-3-60-5-1-6-500	20.54	20.76	0.99	130	250-3-60-5-1-8-500	31.52	32.64	0.97
59	200-3-75-3-1-6-500	20.82	20.76	1.00*	131	250-3-75-3-1-8-500	31.81	32.64	0.97
60	200-3-75-5-1-6-500	20.62	20.76	0.99	132	250-3-75-5-1-8-500	31.45	32.64	0.96
61	200-3-60-3-2-6-500	20.18	20.76	0.97	133	250-3-60-3-2-8-500	31.06	32.64	0.95
62	200-3-60-5-2-6-500	19.93	20.76	0.96	134	250-3-60-5-2-8-500	30.80	32.64	0.94
63	200-3-75-3-2-6-500	20.28	20.76	0.98	135	250-3-75-3-2-8-500	31.12	32.64	0.95
64	200-3-75-5-2-6-500	19.96	20.76	0.96	136	250-3-75-5-2-8-500	30.76	32.64	0.94
65	200-3-60-3-1-8-500	20.33	20.76	0.98	137	250-3-60-3-1-12-500	30.78	32.64	0.94
66	200-3-60-5-1-8-500	20.13	20.76	0.97	138	250-3-60-5-1-12-500	30.44	32.64	0.93
67	200-3-75-3-1-8-500	20.36	20.76	0.98	139	250-3-75-3-1-12-500	30.71	32.64	0.94
68	200-3-75-5-1-8-500	20.11	20.76	0.97	140	250-3-75-5-1-12-500	30.29	32.64	0.93
69	200-3-60-3-2-8-500	19.53	20.76	0.94	141	250-3-60-3-2-12-500	29.62	32.64	0.91
70	200-3-60-5-2-8-500	19.22	20.76	0.93	142	250-3-60-5-2-12-500	29.01	32.64	0.89
71	200-3-75-3-2-8-500	19.61	20.76	0.94	143	250-3-75-3-2-12-500	29.52	32.64	0.90
72	200-3-75-5-2-8-500	19.28	20.76	0.93	144	250-3-75-5-2-12-500	28.32	32.64	0.87

Note: M_{slots} = bending capacity of slotted web channel, M_{solid} = bending capacity of solid web channel, * = numerical errors

Table 10: Parametric study results for f_y = 600 MPa

No	Channels with Slotted Webs	M_{slots} (kNm)	M_{solid} (kNm)	M_{slots} / M_{solid}	No	Channels with Slotted Webs	M_{slots} (kNm)	M_{solid} (kNm)	M_{slots} / M_{solid}
1	150-1-60-3-1-6-600	3.85	4.06	0.95	73	250-1-60-3-1-6-600	6.05	6.33	0.95
2	150-1-60-5-1-6-600	3.75	4.06	0.92	74	250-1-60-5-1-6-600	6.13	6.33	0.97
3	150-1-75-3-1-6-600	3.72	4.06	0.92	75	250-1-75-3-1-6-600	6.12	6.33	0.97
4	150-1-75-5-1-6-600	3.58	4.06	0.88	76	250-1-75-5-1-6-600	6.09	6.33	0.96
5	150-1-60-3-2-6-600	3.44	4.06	0.85	77	250-1-60-3-2-6-600	6.18	6.33	0.98
6	150-1-60-5-2-6-600	3.29	4.06	0.81	78	250-1-60-5-2-6-600	6.14	6.33	0.97
7	150-1-75-3-2-6-600	3.35	4.06	0.82	79	250-1-75-3-2-6-600	6.11	6.33	0.97
8	150-1-75-5-2-6-600	3.19	4.06	0.78	80	250-1-75-5-2-6-600	6.07	6.33	0.96
9	150-2-60-3-1-6-600	10.04	10.80	0.93	81	250-1-60-3-1-8-600	6.22	6.33	0.98
10	150-2-60-5-1-6-600	9.84	10.80	0.91	82	250-1-60-5-1-8-600	6.18	6.33	0.98
11	150-2-75-3-1-6-600	9.72	10.80	0.90	83	250-1-75-3-1-8-600	6.16	6.33	0.97
12	150-2-75-5-1-6-600	9.51	10.80	0.88	84	250-1-75-5-1-8-600	6.12	6.33	0.97
13	150-2-60-3-2-6-600	9.51	10.80	0.88	85	250-1-60-3-2-8-600	6.12	6.33	0.97
14	150-2-60-5-2-6-600	9.13	10.80	0.84	86	250-1-60-5-2-8-600	6.07	6.33	0.96
15	150-2-75-3-2-6-600	9.19	10.80	0.85	87	250-1-75-3-2-8-600	6.05	6.33	0.96
16	150-2-75-5-2-6-600	8.61	10.80	0.80	88	250-1-75-5-2-8-600	5.88	6.33	0.93
17	150-3-60-3-1-6-600	15.94	16.91	0.94	89	250-1-60-3-1-12-600	6.05	6.33	0.96
18	150-3-60-5-1-6-600	15.69	16.91	0.93	90	250-1-60-5-1-12-600	6.00	6.33	0.95
19	150-3-75-3-1-6-600	16.16	16.91	0.96	91	250-1-75-3-1-12-600	5.97	6.33	0.94
20	150-3-75-5-1-6-600	15.90	16.91	0.94	92	250-1-75-5-1-12-600	5.93	6.33	0.94
21	150-3-60-3-2-6-600	15.35	16.91	0.91	93	250-1-60-3-2-12-600	5.78	6.33	0.91
22	150-3-60-5-2-6-600	14.90	16.91	0.88	94	250-1-60-5-2-12-600	5.69	6.33	0.90
23	150-3-75-3-2-6-600	15.54	16.91	0.92	95	250-1-75-3-2-12-600	5.66	6.33	0.89
24	150-3-75-5-2-6-600	15.04	16.91	0.89	96	250-1-75-5-2-12-600	5.60	6.33	0.88
25	200-1-60-3-1-6-600	5.49	5.37	1.02*	97	250-2-60-3-1-6-600	20.98	21.22	0.99
26	200-1-60-5-1-6-600	5.45	5.37	1.01*	98	250-2-60-5-1-6-600	20.93	21.22	0.99
27	200-1-75-3-1-6-600	5.36	5.37	1.00*	99	250-2-75-3-1-6-600	20.82	21.22	0.98
28	200-1-75-5-1-6-600	5.34	5.37	0.99	100	250-2-75-5-1-6-600	20.68	21.22	0.97
29	200-1-60-3-2-6-600	5.36	5.37	1.00*	101	250-2-60-3-2-6-600	20.94	21.22	0.99
30	200-1-60-5-2-6-600	5.22	5.37	0.97	102	250-2-60-5-2-6-600	20.91	21.22	0.99
31	200-1-75-3-2-6-600	5.18	5.37	0.96	103	250-2-75-3-2-6-600	20.80	21.22	0.98
32	200-1-75-5-2-6-600	5.11	5.37	0.95	104	250-2-75-5-2-6-600	20.71	21.22	0.98
33	200-1-60-3-1-8-600	5.37	5.37	1.00*	105	250-2-60-3-1-8-600	20.97	21.22	0.99
34	200-1-60-5-1-8-600	5.33	5.37	0.99	106	250-2-60-5-1-8-600	20.93	21.22	0.99
35	200-1-75-3-1-8-600	5.36	5.37	1.00*	107	250-2-75-3-1-8-600	20.79	21.22	0.98
36	200-1-75-5-1-8-600	5.29	5.37	0.98	108	250-2-75-5-1-8-600	20.72	21.22	0.98
37	200-1-60-3-2-8-600	5.09	5.37	0.95	109	250-2-60-3-2-8-600	20.80	21.22	0.98
38	200-1-60-5-2-8-600	4.94	5.37	0.92	110	250-2-60-5-2-8-600	20.69	21.22	0.98
39	200-1-75-3-2-8-600	4.91	5.37	0.91	111	250-2-75-3-2-8-600	20.54	21.22	0.97
40	200-1-75-5-2-8-600	4.74	5.37	0.88	112	250-2-75-5-2-8-600	20.49	21.22	0.97
41	200-2-60-3-1-6-600	14.30	14.57	0.98	113	250-2-60-3-1-12-600	20.59	21.22	0.97
42	200-2-60-5-1-6-600	14.17	14.57	0.97	114	250-2-60-5-1-12-600	20.49	21.22	0.97
43	200-2-75-3-1-6-600	14.04	14.57	0.96	115	250-2-75-3-1-12-600	20.38	21.22	0.96
44	200-2-75-5-1-6-600	13.85	14.57	0.95	116	250-2-75-5-1-12-600	20.04	21.22	0.94
45	200-2-60-3-2-6-600	13.90	14.57	0.95	117	250-2-60-3-2-12-600	19.75	21.22	0.93
46	200-2-60-5-2-6-600	13.73	14.57	0.94	118	250-2-60-5-2-12-600	18.73	21.22	0.88
47	200-2-75-3-2-6-600	13.59	14.57	0.93	119	250-2-75-3-2-12-600	18.85	21.22	0.89
48	200-2-75-5-2-6-600	13.40	14.57	0.92	120	250-2-75-5-2-12-600	17.74	21.22	0.84
49	200-2-60-3-1-8-600	14.05	14.57	0.96	121	250-3-60-3-1-6-600	36.01	36.73	0.98
50	200-2-60-5-1-8-600	13.88	14.57	0.95	122	250-3-60-5-1-6-600	35.88	36.73	0.98
51	200-2-75-3-1-8-600	13.74	14.57	0.94	123	250-3-75-3-1-6-600	35.39	36.73	0.96
52	200-2-75-5-1-8-600	13.54	14.57	0.93	124	250-3-75-5-1-6-600	35.39	36.73	0.96
53	200-2-60-3-2-8-600	13.48	14.57	0.93	125	250-3-60-3-2-6-600	35.57	36.73	0.97
54	200-2-60-5-2-8-600	13.22	14.57	0.91	126	250-3-60-5-2-6-600	35.39	36.73	0.96
55	200-2-75-3-2-8-600	13.12	14.57	0.90	127	250-3-75-3-2-6-600	35.39	36.73	0.96
56	200-2-75-5-2-8-600	12.86	14.57	0.88	128	250-3-75-5-2-6-600	35.39	36.73	0.96
57	200-3-60-3-1-6-600	23.54	23.68	0.99	129	250-3-60-3-1-8-600	35.82	36.73	0.98

58	200-3-60-5-1-6-600	23.39	23.68	0.99	130	250-3-60-5-1-8-600	35.57	36.73	0.97
59	200-3-75-3-1-6-600	23.71	23.68	1.00*	131	250-3-75-3-1-8-600	35.39	36.73	0.96
60	200-3-75-5-1-6-600	23.46	23.68	0.99	132	250-3-75-5-1-8-600	35.39	36.73	0.96
61	200-3-60-3-2-6-600	22.95	23.68	0.97	133	250-3-60-3-2-8-600	35.05	36.73	0.95
62	200-3-60-5-2-6-600	22.66	23.68	0.96	134	250-3-60-5-2-8-600	35.39	36.73	0.96
63	200-3-75-3-2-6-600	23.06	23.68	0.97	135	250-3-75-3-2-8-600	35.39	36.73	0.96
64	200-3-75-5-2-6-600	22.67	23.68	0.96	136	250-3-75-5-2-8-600	35.39	36.73	0.96
65	200-3-60-3-1-8-600	23.14	23.68	0.98	137	250-3-60-3-1-12-600	34.75	36.73	0.95
66	200-3-60-5-1-8-600	22.91	23.68	0.97	138	250-3-60-5-1-12-600	35.57	36.73	0.97
67	200-3-75-3-1-8-600	23.16	23.68	0.98	139	250-3-75-3-1-12-600	35.39	36.73	0.96
68	200-3-75-5-1-8-600	22.86	23.68	0.97	140	250-3-75-5-1-12-600	35.39	36.73	0.96
69	200-3-60-3-2-8-600	22.18	23.68	0.94	141	250-3-60-3-2-12-600	33.36	36.73	0.91
70	200-3-60-5-2-8-600	21.81	23.68	0.92	142	250-3-60-5-2-12-600	35.39	36.73	0.96
71	200-3-75-3-2-8-600	22.23	23.68	0.94	143	250-3-75-3-2-12-600	35.39	36.73	0.96
72	200-3-75-5-2-8-600	21.83	23.68	0.92	144	250-3-75-5-2-12-600	35.39	36.73	0.96

Note: M_{slots} = bending capacity of slotted web channel, M_{solid} = bending capacity of solid web channel, * = numerical errors

5 Proposed design rules for distortional buckling

This section aims to improve the available Direct Strength Method (DSM) based distortional buckling design equations. DSM is an alternative design method and the ultimate capacities can be determined from the elastic buckling and yielding capacities. North American specification for design of cold-formed structural members, AISI S100 [27], and Australian and New Zealand Standard for cold-formed steel structures, AS/NZ 4600 [28] provide the DSM design guidelines to predict the flexural capacity of CFS beams subject to local buckling and distortional buckling. The ultimate bending capacity for distortional buckling (M_{bd}) can be determined from Eqs. 1 and 2.

For $\lambda_d \leq 0.673$, $$M_{bd} = M_y \tag{1}$$

For $\lambda_d > 0.673$, $$M_{bd} = \left[1 - 0.22\left(\frac{M_{od}}{M_y}\right)^{0.5}\right]\left(\frac{M_{od}}{M_y}\right)^{0.5} M_y \tag{2}$$

where $\lambda_d = \sqrt{M_y/M_{od}}$, λ_d is the non-dimensional slenderness to calculate M_{bd}, M_y is the yielding moment which is the product of elastic section modulus (Z) of the section and yield strength and M_{od} is the elastic distortional buckling moment.

The latest version of both AISI S100 [27] and AS/ NZ 4600 [28] has the provision for inelastic reserve capacity for distortional buckling to account higher compressive strains in symmetric CFS beams. Therefore, the inelastic reserve capacity for distortional buckling can be determined for the CFS sections symmetric about the axis of bending or sections with the first yield in compression using Eq. 3.

For $\lambda_d \leq 0.673$, $$M_{bd} = M_y + \left(1 - \frac{1}{C_{yd}^2}\right)\left(M_p - M_y\right) \tag{3}$$

Where M_p is the plastic moment which is the product of plastic section modulus (S) and yield strength (fy) and $c_{yd} = \sqrt{0.673/\lambda_d} \leq 3$.

The ultimate bending capacity prediction for distortional buckling using the current DSM equations (Eqs. 1, 2 and 3) is plotted in Fig. 22. It is essential to calculate the plastic moment (M_p) to plot the inelastic research bending capacity. Therefore, CFS solid sections were analysed to determine the elastic (Z) and plastic section modulus (S) to calculate the shape factor (S/Z) which is equal to the M_p/M_y. The elastic section modulus was obtained from the finite strip method-based software THIN-WALL-2 [29]. Table 7 presents the shape factor values for the nine CFS solid web channels. The mean shape factor value for CFS solid web channels is 1.26 while the minimum value for the shape factor is 1.21. Therefore, as a conservative approach, 1.21 was selected for the analysis of the results of the parametric study. Fig. 22 is also plotted with the distortional buckling test results of CFS beams reported in Yu and Schafer [10] and Pham and Hancock [25]. The ultimate bending capacities for distortional buckling of 27 CFS solid channels obtained from the FE analyses are plotted in the DSM curve (see Fig. 23). These FE results for the CFS beams with solid web are fitting well with the DSM curve for distortional buckling.

AISI S100 [27] and AS/NZ 4600 [28] provides DSM based design guidelines to predict the ultimate bending capacity of the CFS beams with rectangular web holes. These provisions cannot be applicable for this staggered slotted perforated CFS beams due to the arrangement and patterns of the holes. Therefore, a simple approach is chosen where a reduction factor (q_s) was proposed as a function of influencing parameters considered in the parametric study. The ultimate bending capacity of the staggered slotted perforated CFS beams subject to distortional buckling (M_{slots}) can be calculated by applying q_s to its corresponding bending capacity of the solid CFS beams (M_{solid}) as mentioned in Eq. 4.

$$M_{slots} = M_{solid} \times q_s \tag{4}$$

Using the comprehensive ultimate bending capacity data obtained for the parametric study (432 results), an appropriate reduction factor equation was proposed considering all influencing parameters. Eq. 5 gives the proposed reduction factor equation. This equation was developed and optimised through a classic genetic algorithm and using the Generalised Reduced Gradient (GRG) solving method. The objective function was aimed to minimise the COV of the q_s(FE)/q_s(proposed) ratios of the 432 results while maintaining the mean value equal to unity. The optimisation resulted in a COV of 0.04, thus defines the satisfactory accuracy of the proposed reduction factor equation. Fig. 24 depicts the comparison of the reduction factor obtained from FE analysis and proposed equation.

$$q_s = 1 - \frac{\left[\frac{B_l}{B_f}\right]^{1.077}\left[\frac{D}{t}\right]^{0.065}\left[\frac{L_{sl}}{100}\right]^{1.023}\left[\frac{W_{sl}}{9.5}\right]^{0.555}\left[\frac{N}{n}\right]^{0.502}}{\left[\frac{f_y}{250}\right]^{0.004}} \quad (5)$$

The proposed reduction factor q_s can be adopted into the DSM equations for distortional buckling of CFS beams (Eq.2 and 3). The modified DSM equations with the reduction factor q_s to predict the ultimate bending capacity of CFS beams with staggered slotted perforation are provided in Eqs.6 and 7.

For $\lambda_d > 0.673,\quad M_{bd,slots} = \left[\left[1 - 0.22\left(\frac{M_{od}}{M_y}\right)^{0.5}\right]\left(\frac{M_{od}}{M_{y,}}\right)^{0.5} M_y\right] q_s$ (6)

For $\lambda_d \leq 0.673,\quad M_{bd,slots} = \left[M_y + \left(1 - \frac{1}{C_{yd}^2}\right)\left(M_p - M_y\right)\right] q_s$ (7)

Where q_s can be substituted from Eq. 5.

Fig. 25 shows bending capacity predictions of the staggered slotted perforated CFS beams obtained from the modified DSM equations (Eq.6 and 7) for distortional buckling. All 432 points plotted in Fig. 25 reveals a satisfactory agreement with the DSM curve. Therefore, these modified DSM based design equations are suitable to predict the ultimate bending capacity of staggered slotted perforated CFS beams subject to distortional buckling accurately.

6 Concluding remarks

CFS beams with staggered slotted perforations are widely used in steel buildings to enhance the thermal performance. However, the effect of incorporating staggered slotted perforations on structural performance is not fully studied yet. Therefore, this paper has presented a comprehensive numerical analysis on staggered slotted perforated CFS flexural members subjected to distortional buckling. A detailed parametric study using 432 models was conducted to generate a wide range of ultimate bending capacity data set of CFS beams with staggered slotted perforations. The results showed that the slotted perforations in the web reduced the ultimate bending capacity up to 23%. Then, the results were used to modify the DSM based design equations to accurately predict the ultimate bending capacity of CFS beams with slotted perforations in accordance with the design rules for the solid-webbed CFS beams. The modified DSM based equations resulted good accuracy in predicting the bending capacities of slotted perforated channels, considering all the influencing parameters. Therefore, the ultimate bending capacity of staggered slotted perforated CFS beams can be reliably calculated using the modified DSM based equations.

Acknowledgements

The authors would like to appreciate the necessary research facilities and technical assistance provided by South Ural State University and Northumbria University.

References

[1] T. Höglund, H. Burstrand, Slotted steel studs to reduce thermal bridges in insulated walls, Thin-Walled Structures. 32 (1998) 81-109. doi:10.1016/s0263-8231(98)00028-7.

[2] R. LaBoube, Development of cost-effective, energy-efficient steel framing: Thermal performance of slit-web steel wall studs, American Iron and Steel Institute, 2006.

[3] J. Lipták-Váradi, Equivalent thermal conductivity of steel girders with slotted web, Periodica Polytechnica Civil Engineering. 54 (2010) 163. doi:10.3311/pp.ci.2010-2.12.

[4] F. Liu, F. Fu, Y. Wang, Q. Liu, Fire performance of non-load-bearing light-gauge slotted steel stud walls, Journal of Constructional Steel Research. 137 (2017) 228-241. doi:10.1016/j.jcsr.2017.06.034.

[5] Kesti, Local and distortional buckling of perforated steel wall studs, PhD, Helsinki University of Technology, 2000.

[6] N. Degtyareva, V. Degtyarev, Experimental investigation of cold-formed steel channels with slotted webs in shear, Thin-Walled Structures. 102 (2016) 30-42. doi:10.1016/j.tws.2016.01.012.

[7] V. Degtyarev, N. Degtyareva, Finite element modeling of cold-formed steel channels with solid and slotted webs in shear, Thin-Walled Structures. 103 (2016) 183-198. doi:10.1016/j.tws.2016.02.016.

[8] N. Degtyareva, P. Gatheeshgar, K. Poologanathan, S. Gunalan, M. Lawson, P. Sunday, Combined bending and shear behaviour of slotted perforated steel channels: Numerical studies, Journal of Constructional Steel Research. 161 (2019) 369-384. doi:10.1016/j.jcsr.2019.07.008.

[9] C. Yu, B. Schafer, Local Buckling Tests on Cold-Formed Steel Beams, Journal Of Structural Engineering. 129 (2003) 1596-1606. doi:10.1061/(asce)0733-9445(2003)129:12(1596).

[10] C. Yu, B. Schafer, Distortional Buckling Tests on Cold-Formed Steel Beams, Journal Of Structural Engineering. 132 (2006) 515-528. doi:10.1061/(asce)0733-9445(2006)132:4(515).

[11] N. Nguyen, T. Fung, B. Young, Strength and Behavior of Cold-Formed Steel Z - Sections Subjected to Major Axis Bending, Journal Of Structural Engineering. 132 (2006) 1632-1640. doi:10.1061/(asce)0733-9445(2006)132:10(1632).

[12] H. Wang, Y. Zhang, Experimental and numerical investigation on cold-formed steel C-section flexural members, Journal of Constructional Steel Research. 65 (2009) 1225-1235. doi:10.1016/j.jcsr.2008.08.007.

[13] C. Yu, B. Schafer, Simulation of cold-formed steel beams in local and distortional buckling with applications to the direct strength method, Journal of Constructional Steel Research. 63 (2007) 581-590. doi:10.1016/j.jcsr.2006.07.008.

[14] R. Siahaan, P. Keerthan, M. Mahendran, Finite element modeling of rivet fastened rectangular hollow flange channel beams subject to local buckling, Engineering Structures. 126 (2016) 311-327. doi:10.1016/j.engstruct.2016.07.004.

[15] R. Siahaan, M. Mahendran, P. Keerthan, Section moment capacity tests of rivet fastened rectangular hollow flange channel beams, Journal Of Constructional Steel Research. 125 (2016) 252-262. doi:10.1016/j.jcsr.2016.06.021.

[16] R. Siahaan, M. Mahendran, P. Keerthan, Section moment capacity tests of rivet fastened rectangular hollow flange channel beams, Journal Of Constructional Steel Research. 125 (2016) 252-262. doi:10.1016/j.jcsr.2016.06.021.

[17] C. Moen, A. Schudlich, A. von der Heyden, Experiments on Cold-Formed Steel C-Section Joists with Unstiffened Web Holes, Journal Of Structural Engineering. 139 (2013) 695-704. doi:10.1061/(asce)st.1943-541x.0000652.

[18] J. Zhao, K. Sun, C. Yu, J. Wang, Tests and direct strength design on cold-formed steel channel beams with web holes, Engineering Structures. 184 (2019) 434-446. doi:10.1016/j.engstruct.2019.01.062.

[19] J. Kesti, Uumasta rei’itetyn seinärangan mitoitustutkimus. Lisensiaatintyö, joka on jätetty opinnäytteenä tarkastettavaksi tekniikan lisensiaatin tutkintoa, Teknillinen Korkeakoulu, 1997. (in Finnish).

[20] N. Degtyareva, Review of Experimental Studies of Cold-Formed Steel Channels with Slotted Webs under Bending, Procedia Engineering. 206 (2017) 875-880. doi:10.1016/j.proeng.2017.10.566.

[21] ANSYS, Commands reference, elements reference, operations guide, Basic Analysis Guide, Theory Reference for ANSYS (2019)

[22] B. Schafer, Z. Li, C. Moen, Computational modelling of cold-formed steel, Thin-Walled Structures. 48 (2010) 752-762. doi:10.1016/j.tws.2010.04.008.

[23] B. Schafer, T. Peköz, Computational modeling of cold-formed steel: characterizing geometric imperfections and residual stresses, Journal of Constructional Steel Research. 47 (1998) 193-210. doi:10.1016/s0143-974x(98)00007-8.

[24] D. Camotim, N. Silvestre, GBT based analysis of the distortional postbuckling behaviour of cold-formed steel Z-section columns and beams, in: Fourth International Conference On Thin-Walled Structures, Loughborough, 2004: pp. 243-250.

[25] C. Pham, G. Hancock, Experimental Investigation and Direct Strength Design of High-Strength, Complex C-Sections in Pure Bending, Journal of Structural Engineering. 139 (2013) 1842-1852. doi:10.1061/(asce)st.1943-541x.0000736.

[26] C. Pham, Direct Strength Method of Design of Cold-Formed Sections in shear, and Combined bending and shear, Ph.D, The University of Sydney, 2010.

[27] American Iron and Steel Institute (AISI), Specifications for the cold-formed steel structural members, cold-formed steel design manual, AISI S100, Washington DC, USA, 2016.

[28] Standards Australia, AS/NZS 4600:2018: Cold-formed steel structures. Sydney, Australia, 2018.

[29] V. V. Nguyen, G. J. Hancock, C. H. Pham, Development of the Thin-Wall-2 program for buckling analysis of thin-walled sections under generalised loading, Proceedings of the eighth international conference on advances in steel structures, Lisbon, Portugal, 2015.

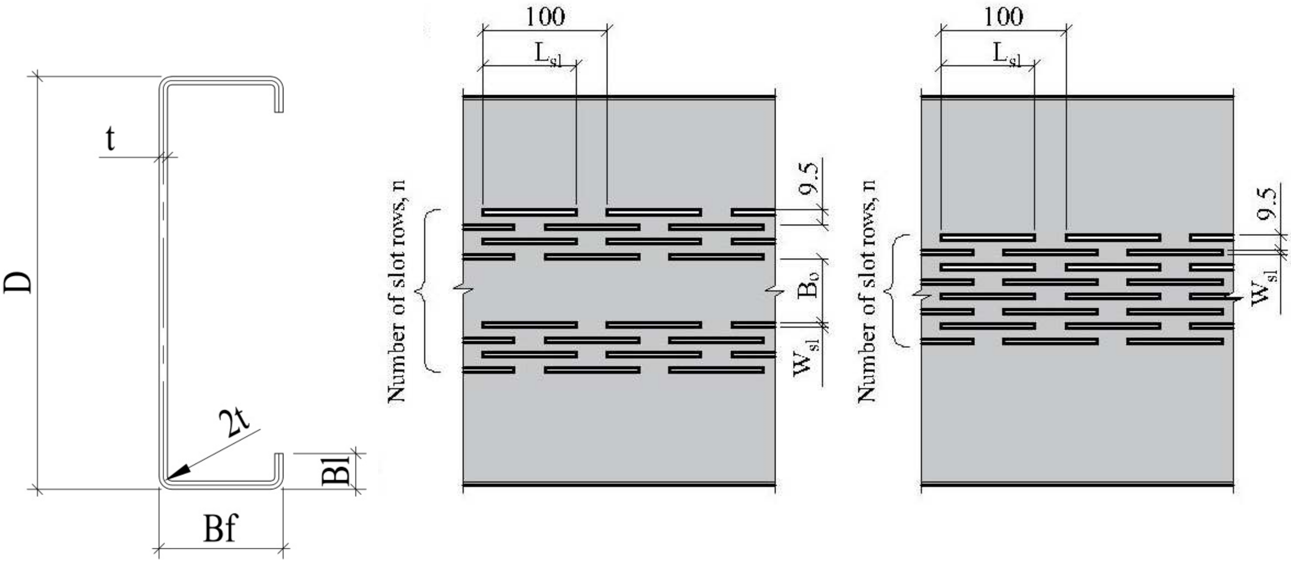

Fig. 1. CFS beams with slotted perforations

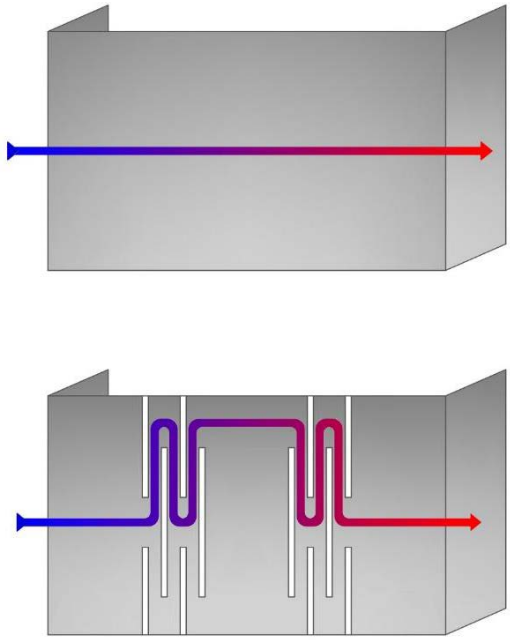

Fig. 2. Heat flow path in solid and slotted web CFS beams

Fig. 3. Application of slotted perforated CFS beams

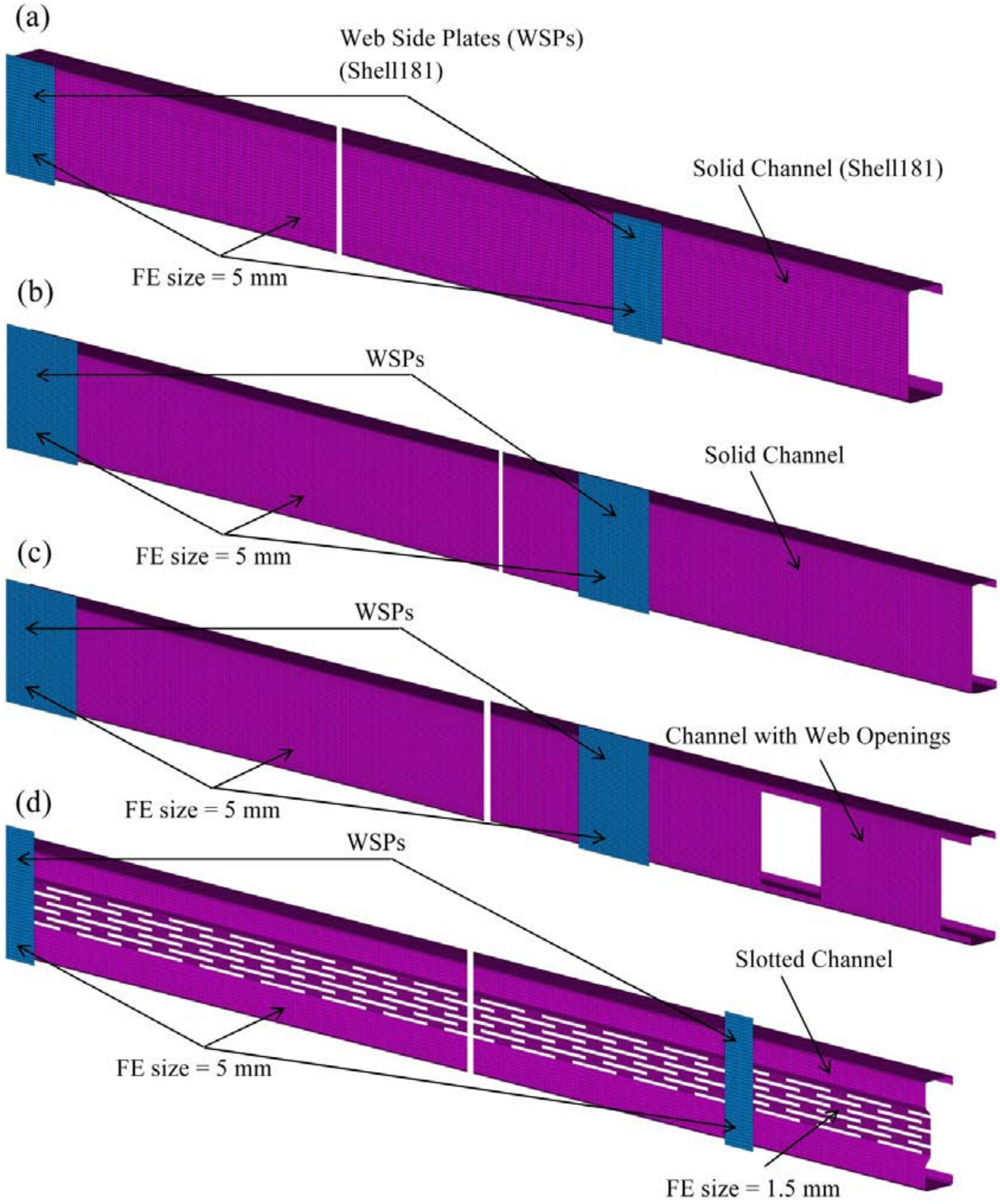

Fig. 4. Developed FE models to validate the test results of: (a) Pham [25]; (b, c) Moen [17]; (d) Kesti [19]

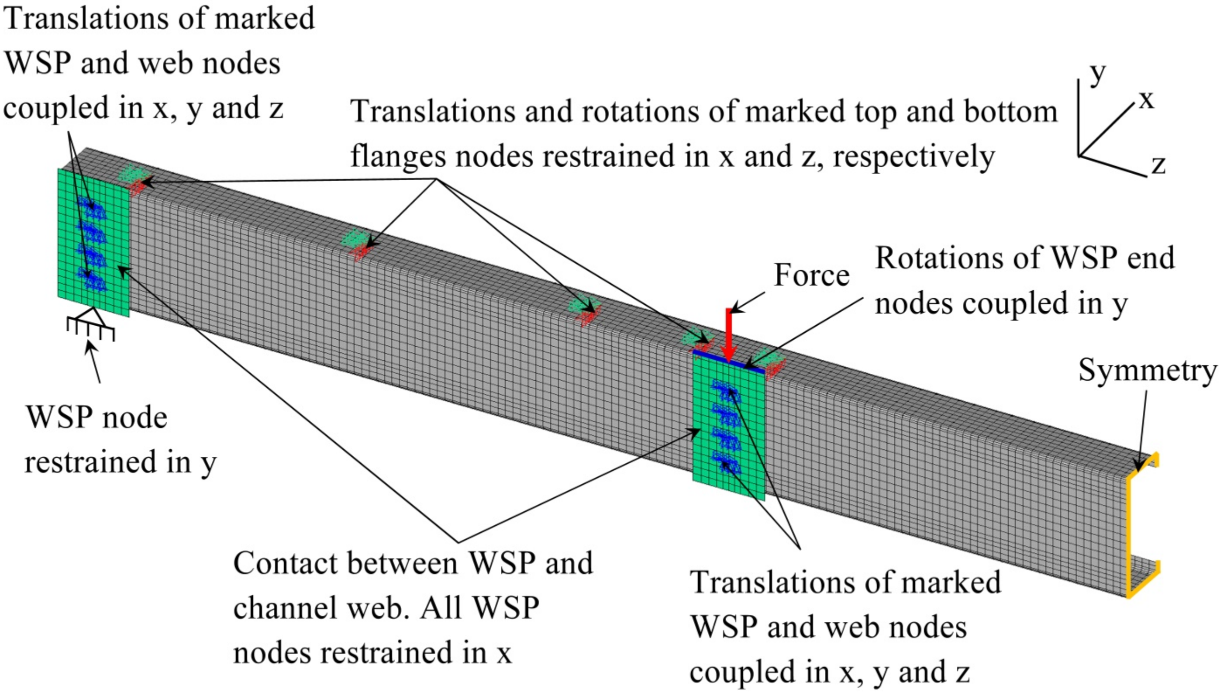

Fig. 5. Simulated boundary conditions in FE model to validate Pham's [25] tests

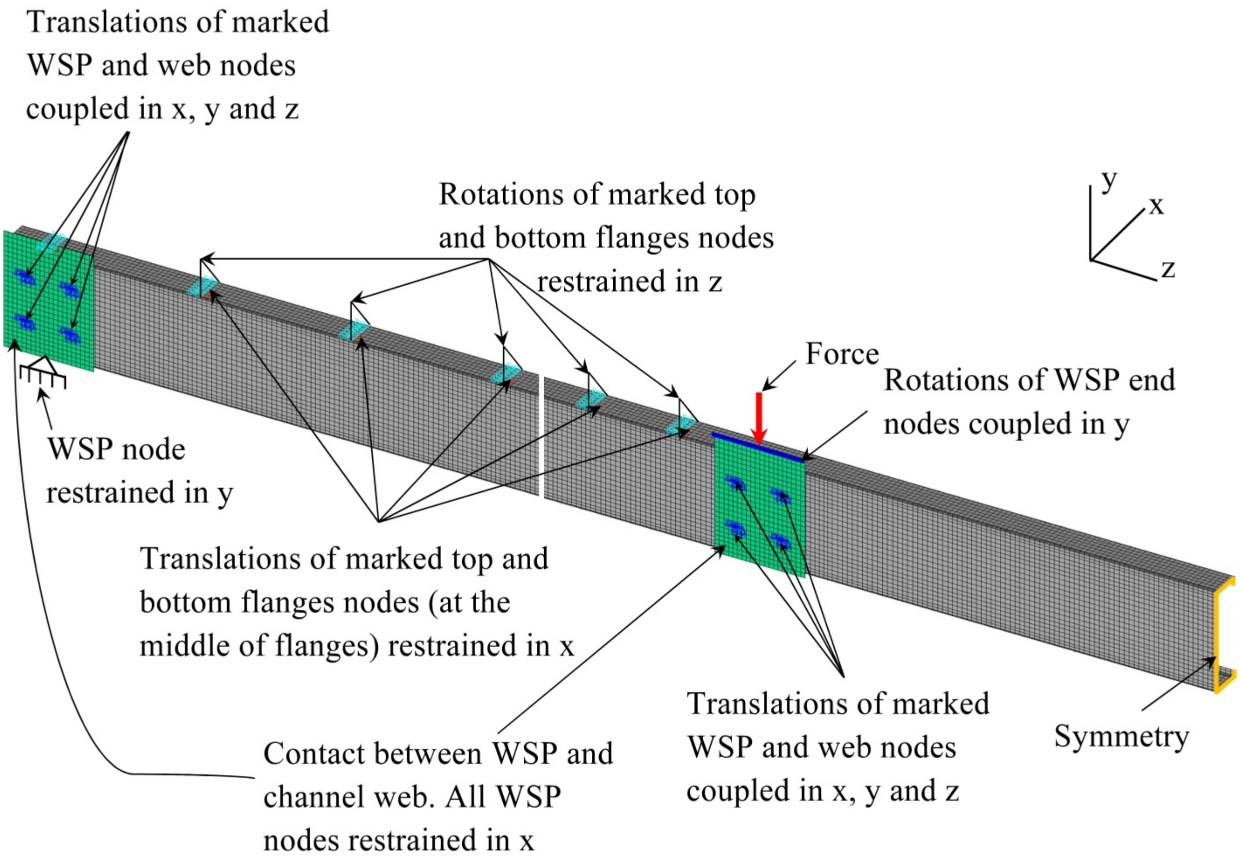

Fig. 6. Simulated boundary conditions in FE model to validate Moen's [17] tests

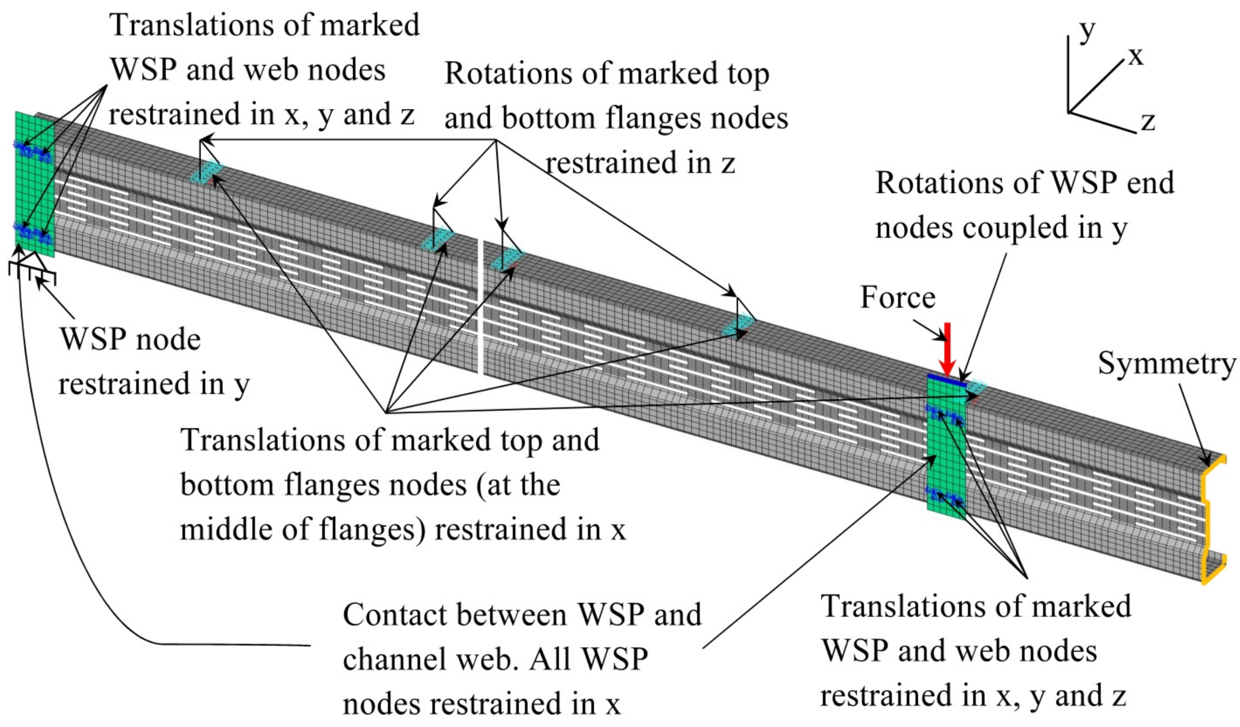

Fig. 7. Simulated boundary conditions in FE model to validate Kesti's [19] tests

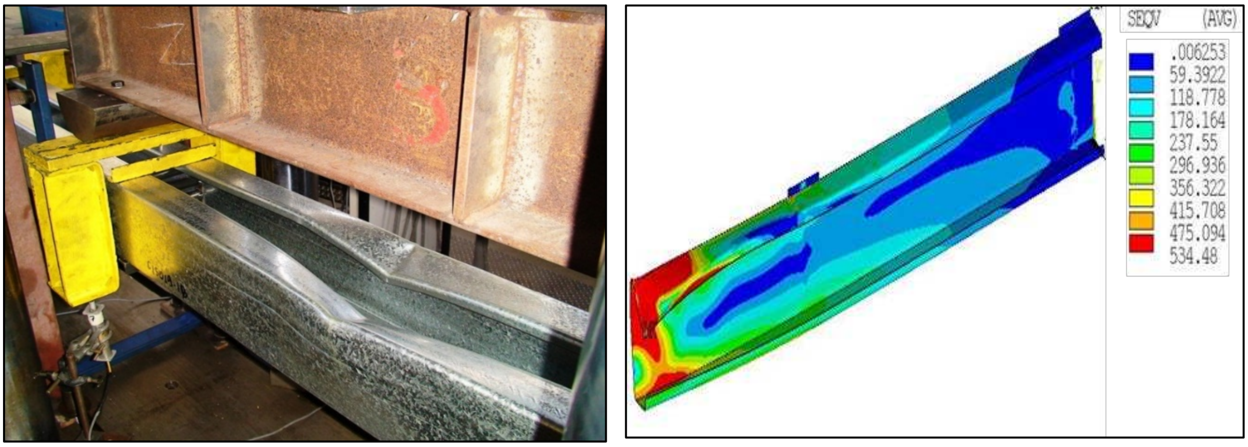

Fig. 8. Failure mode comparison between test [26] and FE models of the tested specimen C15019-Mw and FE model

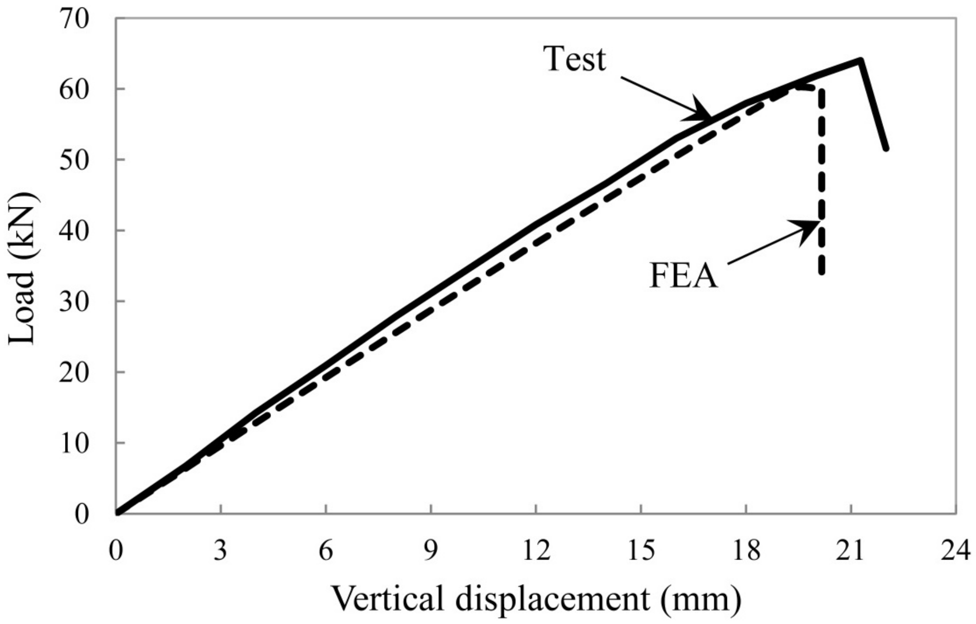

Fig. 9. Load-vertical displacement behaviour obtained for the specimen C15019-Mw from test [25] and FE analysis.

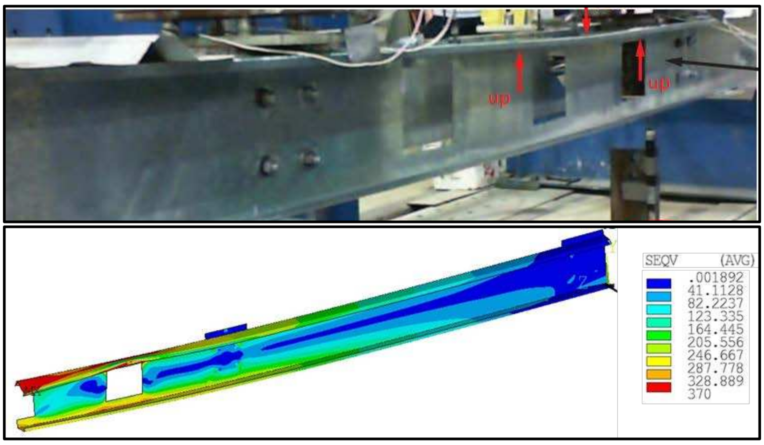

(a) H0.9-3.1

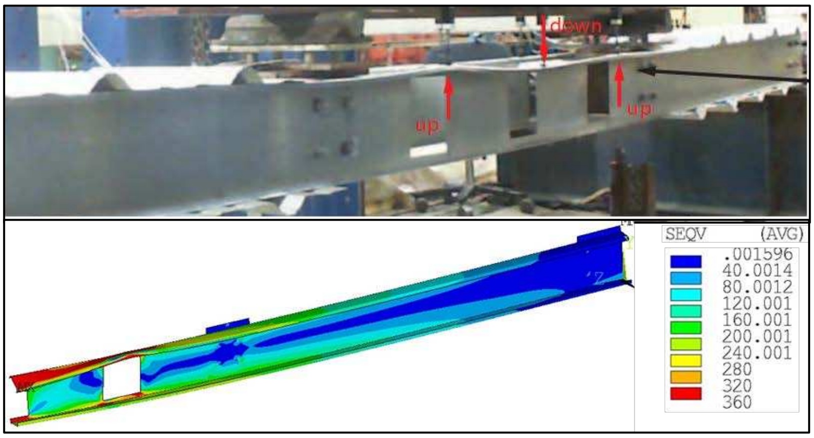

(b) H0.8-1.2

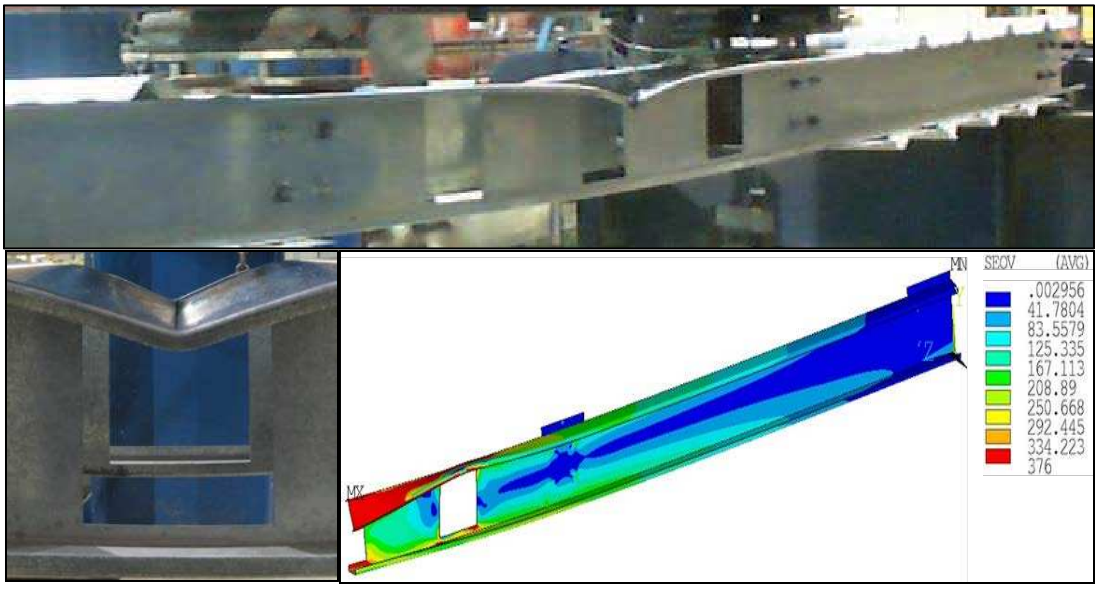

(b) H0.8-3.2

Fig.10. Failure modes comparison between test [17] and FE models

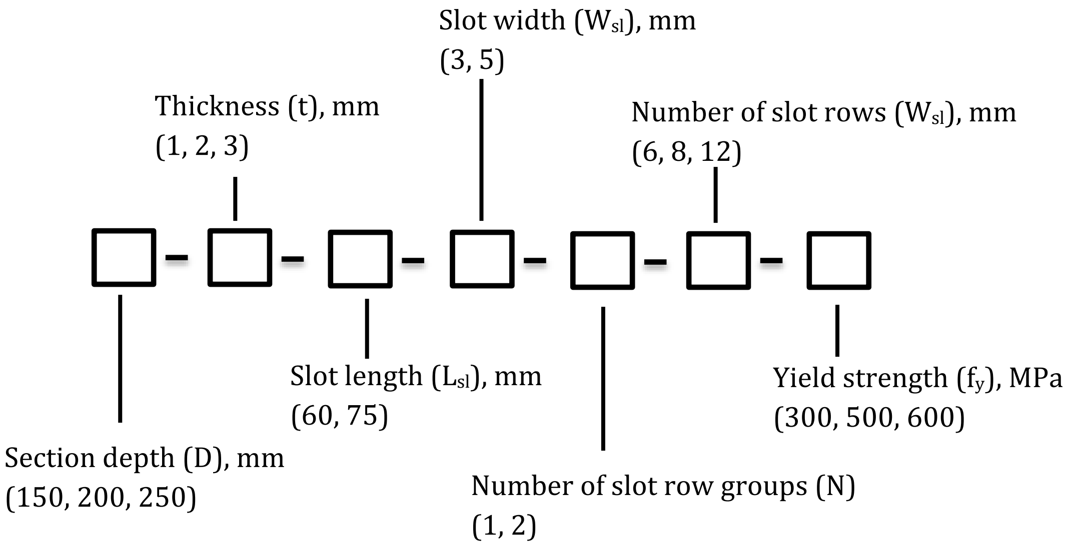

Fig. 11. FE model nomenclature for parametric study

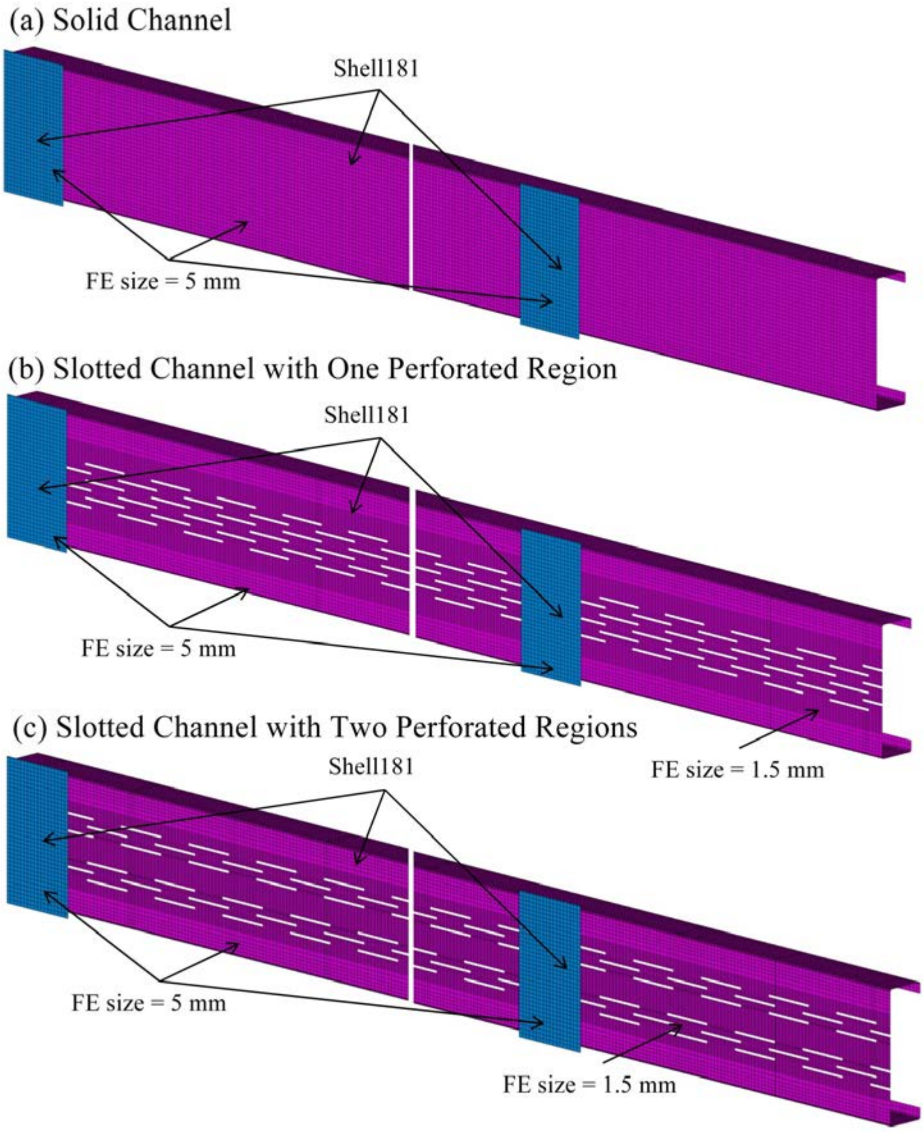

Fig. 12. FE models of 4800 mm long beam with staggered slotted perforations are provided in entire span (for parametric study)

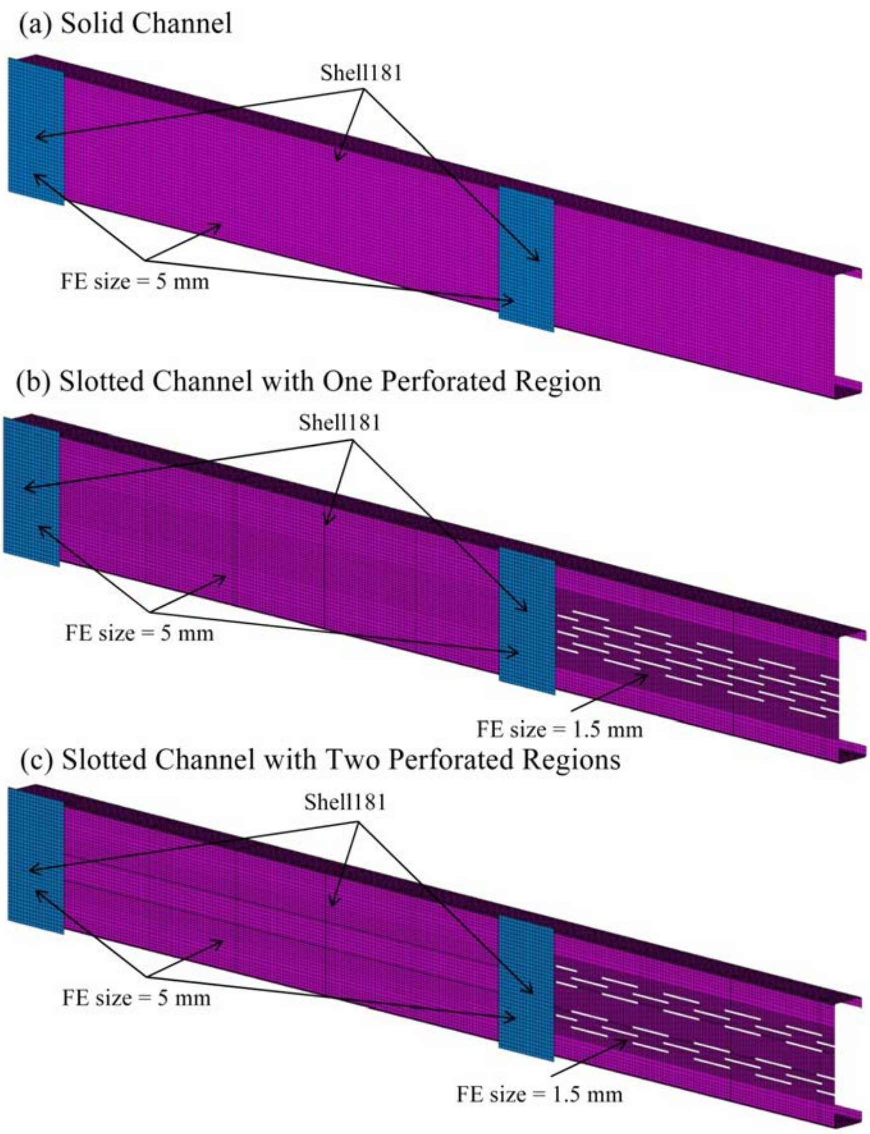

Fig. 13. FE models of 2600 mm long beam with staggered slotted perforations are only provided in the mid-span (for parametric study)

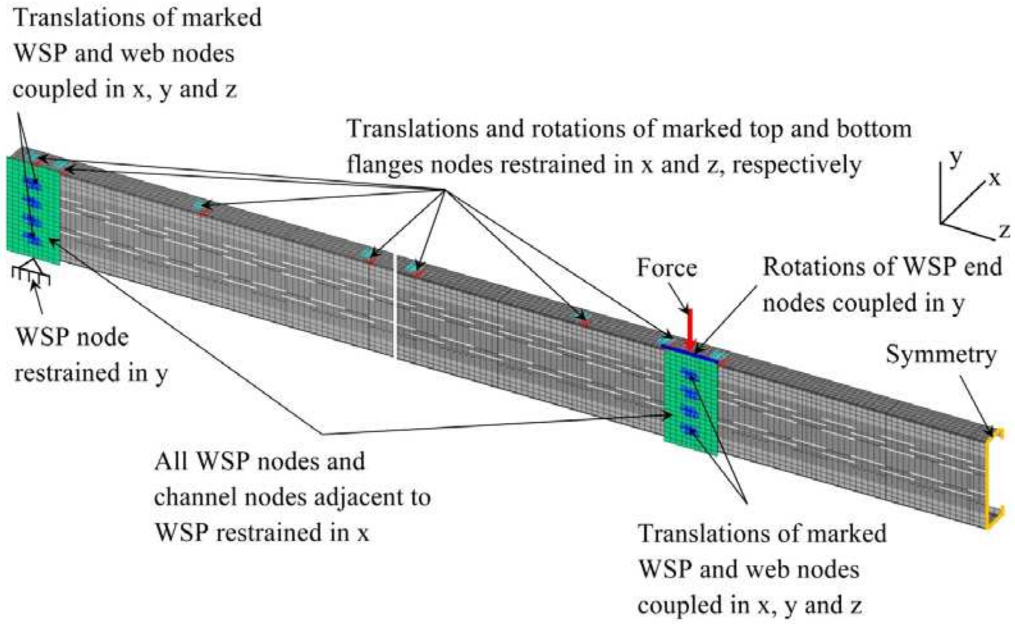

Fig. 14. Boundary conditions for FE models of 4800 mm long beams

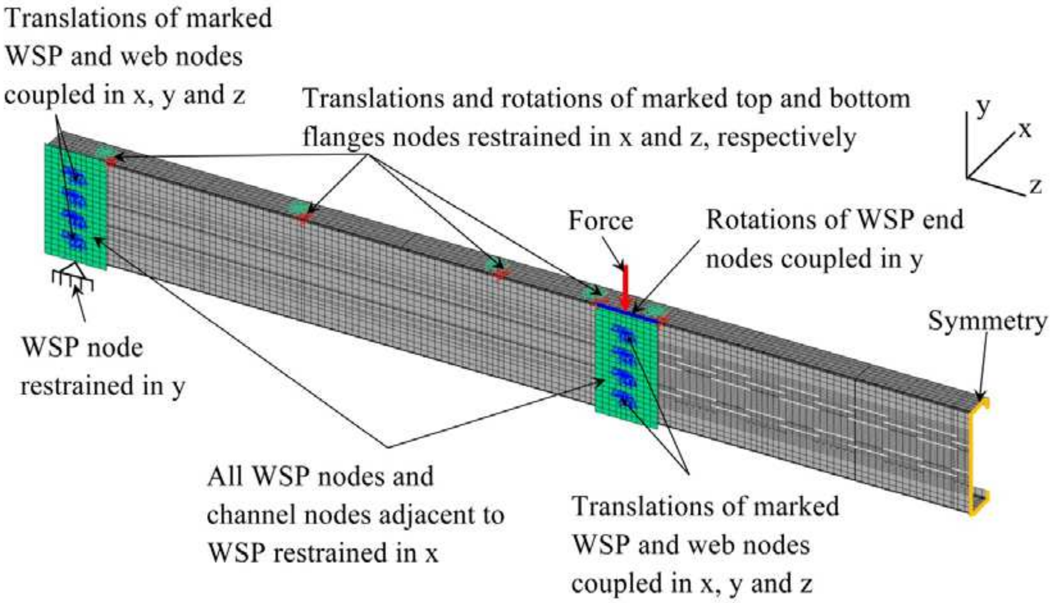

Fig. 15. Boundary conditions for FE models of 2600 mm long beams (for parametric study)

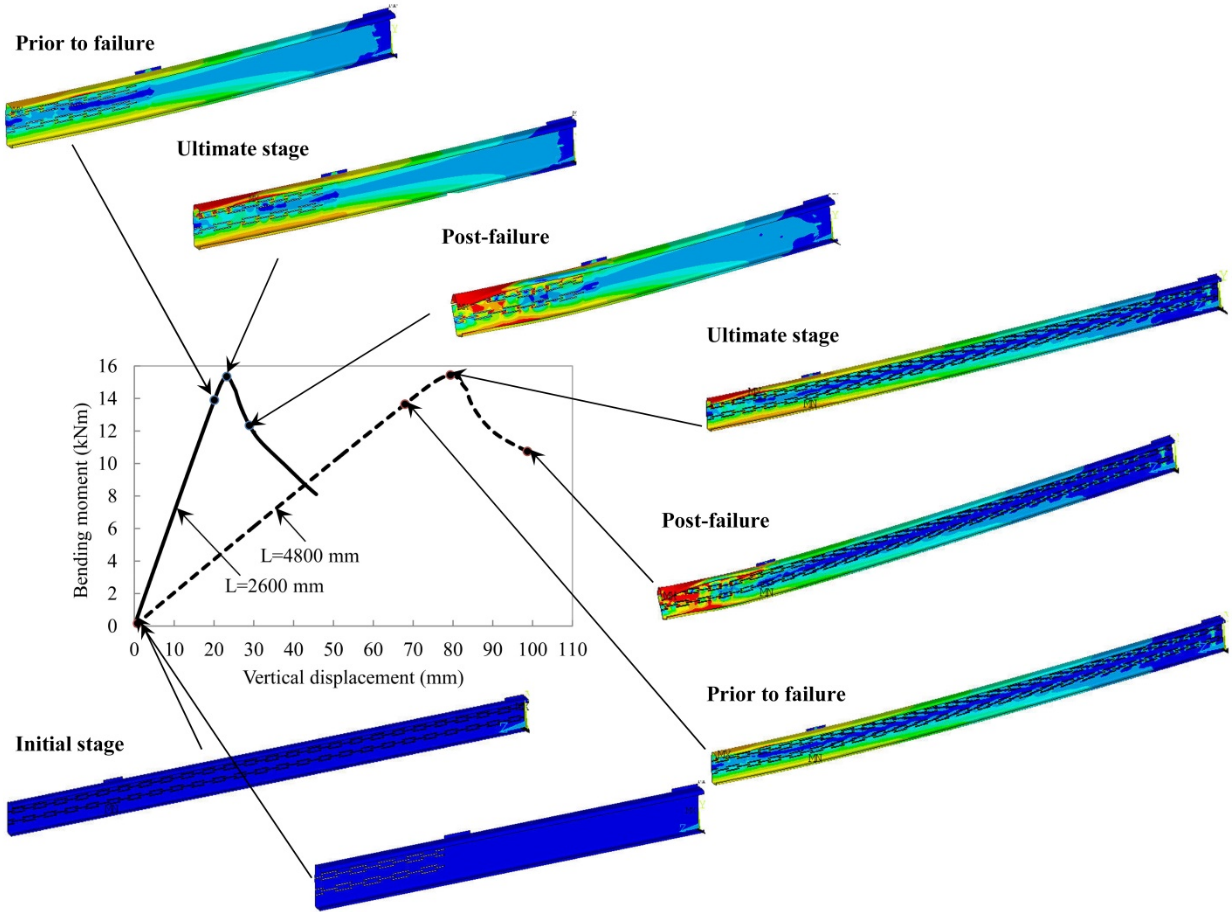

Fig. 16. Load-deflection plot of slotted channel 150-3-60-3-2-6-600 and its behavior at different stages.

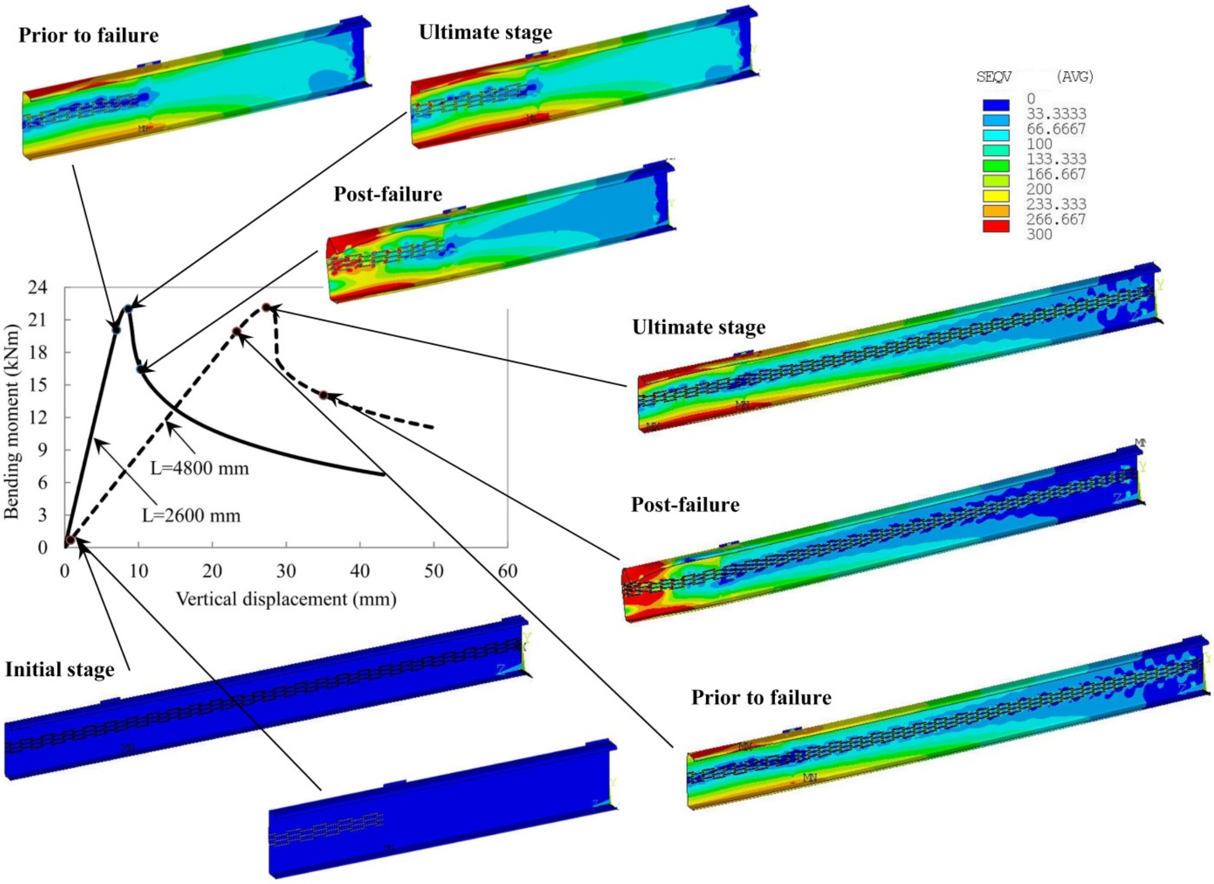

Fig. 17. Load-deflection plot of slotted channel 250-3-60-3-1-6-300 and its behavior at different stages.

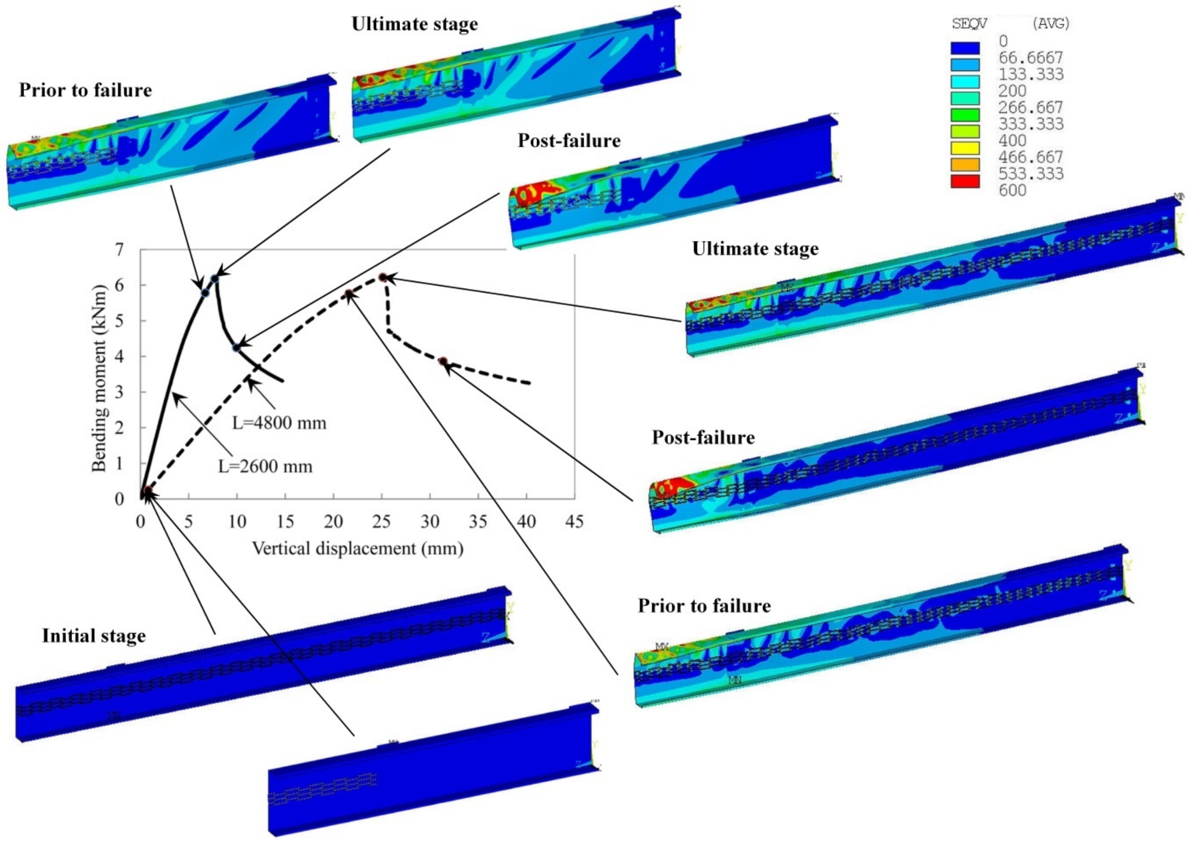

Fig. 18. Load-deflection plot of slotted channel 250-1-60-3-1-6-600 and its behavior at different stages.

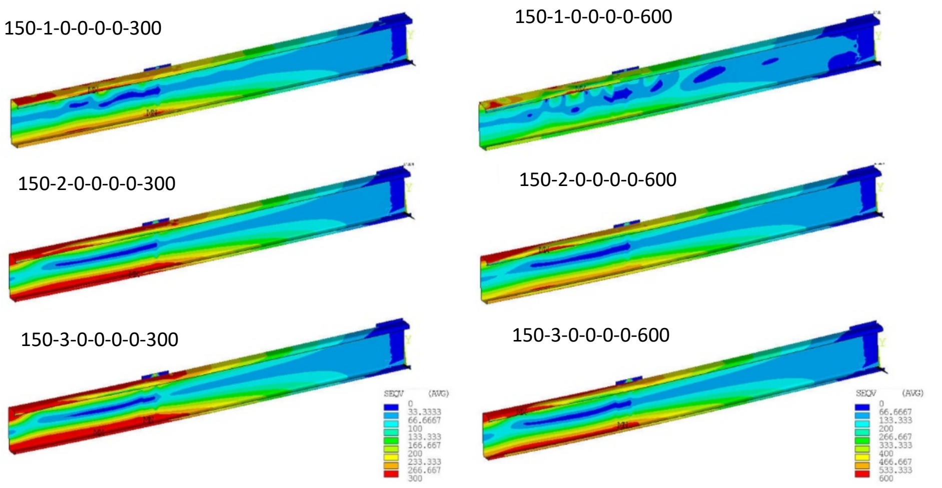

(a) Solid web CFS channels

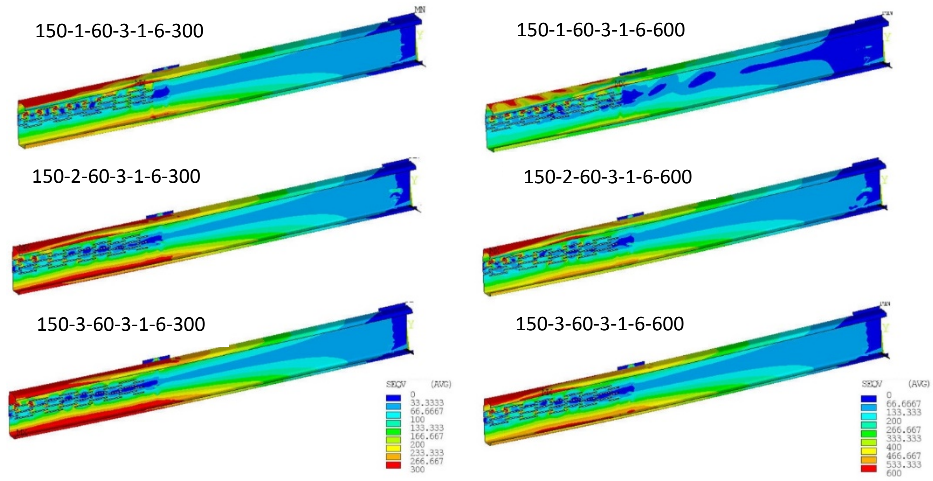

(b) Staggered slotted perforated channels

Fig. 19. Von misses stress failure pattern for 150 mm section depth solid and slotted perforated channels.

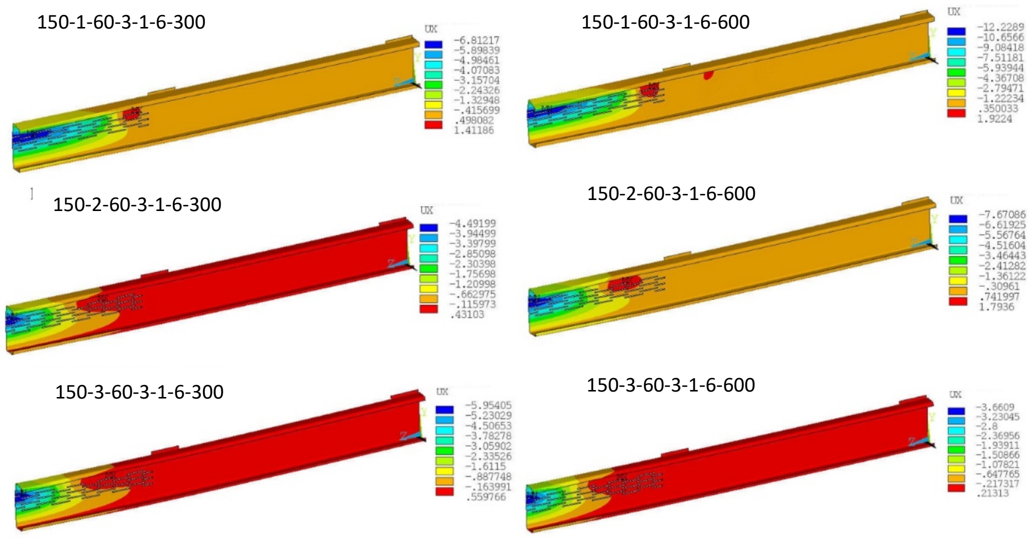

(a) 150 mm section depth CFS channels

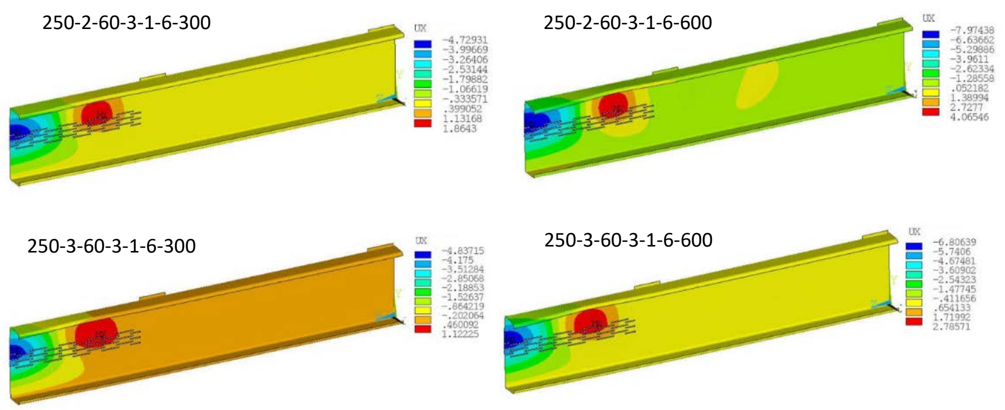

(b) 250 mm section depth CFS channels

Fig. 20. Deformation failure pattern of 150 and 250 mm section depth CFS channels with staggered slotted perforations

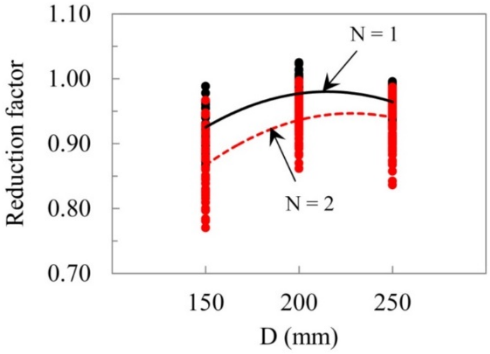

(a) Section depth

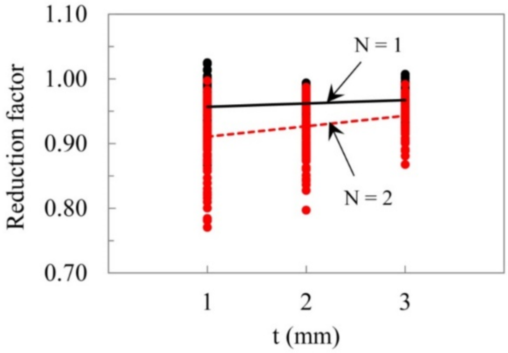

(b) Thickness

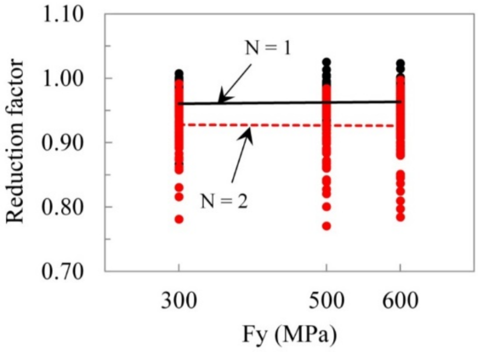

(c) Yield strength

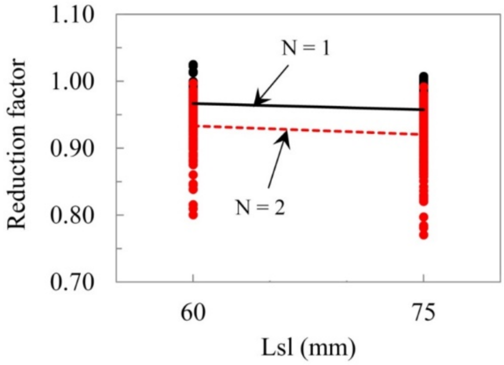

(d) Slot length

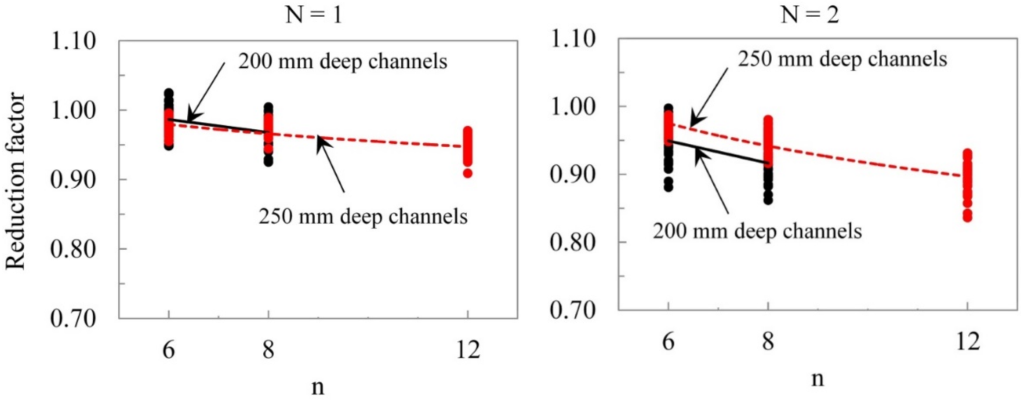

(e) Slot rows and slot row groups

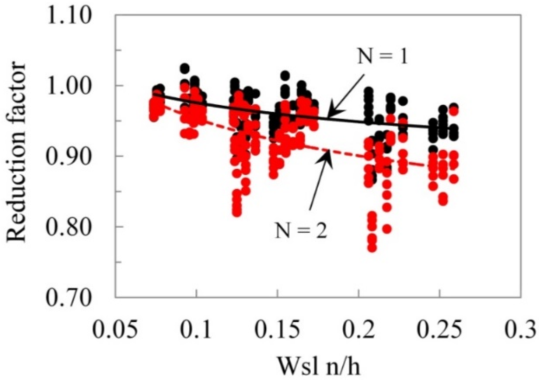

(f) Slot width

Fig. 21. Variation of reduction factor with influencing parameters.

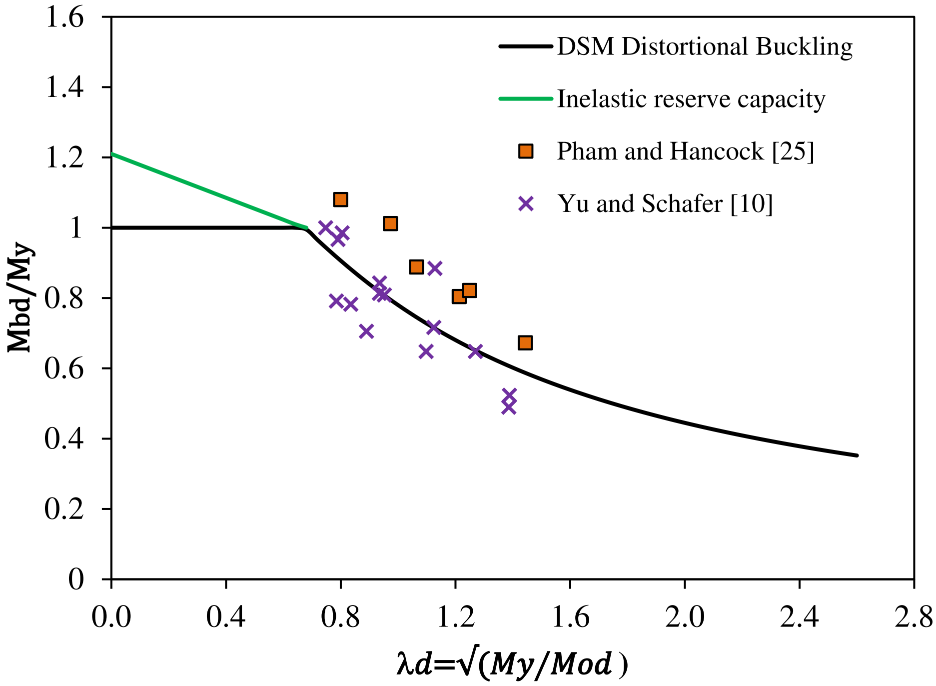

Fig. 22. DSM for distortional buckling and test results [10, 25]

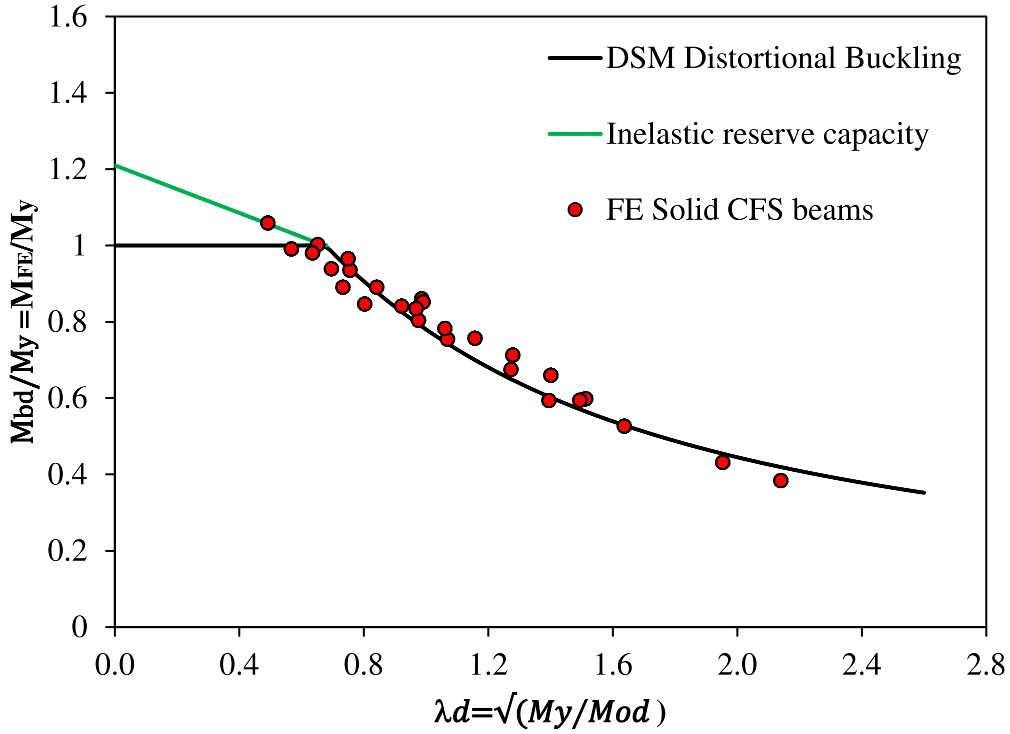

Fig. 23. FE capacity predictions for CFS solid web beams

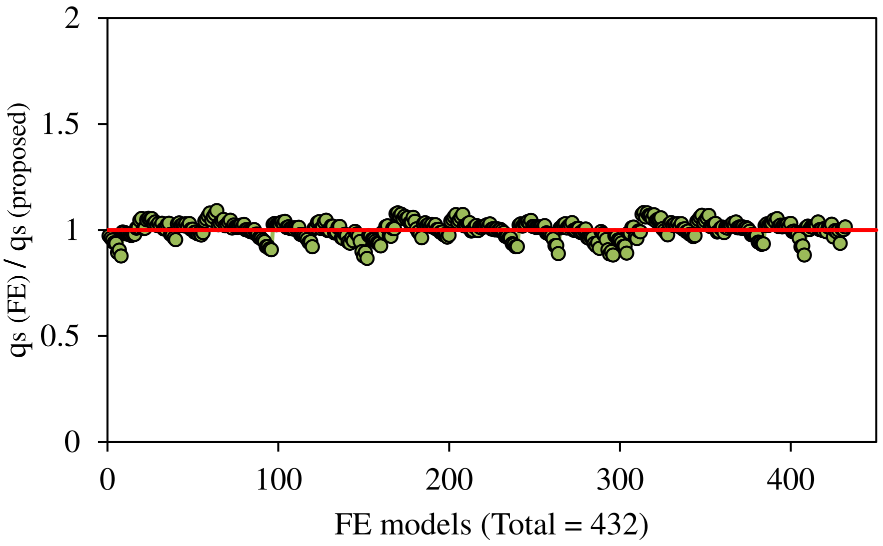

Fig. 24. Comparison of the reduction factor obtained from FE and proposed equation

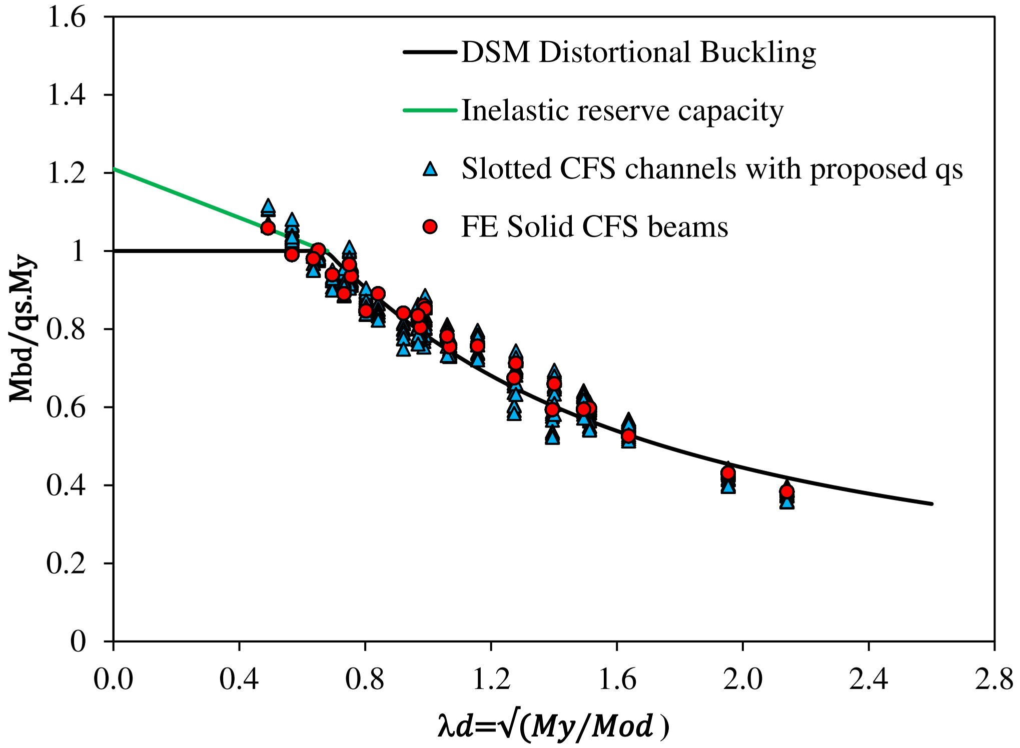

For solid CFS channels, $q_s = 1$ For slotted perforated CFS channels, q_s is from Eq. 5

Fig. 25. Bending capacity predictions for slotted perforated beams with proposed q_s along with corresponding solid web beams